FIRING-RATE RESONANCES IN SMALL NEURONAL NETWORKS

DISSERTATION

zur Erlangung des akademischen Grades
Doctor rerum naturalium (Dr. rer. nat.)
im Fach Biologie

eingereicht an der
Lebenswissenschaftlichen Fakultät
der Humboldt-Universität zu Berlin

von

Dipl.-Biol. Florian Rau

Präsident der Humboldt-Universität zu Berlin
Prof. Dr. Jan-Hendrik Olbertz

Dekan der Lebenswissenschaftlichen Fakultät
Prof. Dr. Richard Lucius

Gutachter/-innen: Prof. Dr. Matthias Hennig
Prof. Dr. Susanne Schreiber
Prof. Dr. Martin Nawrot

Eingereicht am 22. August 2014
Tag der mündlichen Prüfung: 19. Dezember 2014

Zusammenfassung

In vielen Kommunikationssytemen wird Information durch die zeitliche Struktur von Signalen kodiert. Ein neuronales System, welches rhythmische Signale verarbeitet, sollte davon profitieren, seine inhärenten Filtereigenschaften den Frequenzcharakteristika dieser Signale anzupassen. Die Grille *Gryllus bimaculatus* stellt ein einfaches biologisches System dar, für welches nur wenige, spezifische Modulationsfrequenzen verhaltensrelevant sind. Ich habe einzelne Neuronen im peripheren und höheren auditorischen System der Grille hinsichtlich einer möglichen Anpassung auf diese Frequenzen untersucht. Hierfür habe ich extrazelluläre Elektrophysiologie mit verschiedenen Stimulationsparadigmen kombiniert, welche auf amplitudenmodulierten Tönen basierten. Die Analyse der experimentellen Daten ergab, dass bereits in der auditorischen Peripherie einige der untersuchten Neurone Bandpasseigenschaften aufwiesen, da sie verhaltensrelevante Modulationsfrequenzen mit den höchsten Feuerraten beantworteten. Anhand einfacher mathematischer Modelle demonstriere ich, wie weitverbreitete, zellintrinsische und netzwerkbasierte Mechanismen die beobachteten Feuerratenresonanzen erklären könnten. Diese Mechanismen umfassen unterschwellige Resonanz von Membranströmen, aktivitätsabhängige Adaptation, sowie das Zusammenwirken von Exzitation und Inhibition. Ich zeige, wie eine serielle Kombination solcher elementarer Filter die deutliche Selektivität im Verhalten der Grille erklären könnte, ohne dabei auf ein dediziertes Filterelement zurückzugreifen. Allgegenwärtige neuronale Mechanismen könnten demnach eine dezentralisierte Filterkaskade in einem hochspezialisierten und größenbeschränkten neuronalen System begründen.

Abstract

In many communication systems, information is encoded in the temporal pattern of signals. For rhythmic signals that carry information in specific frequency bands, a neuronal system may profit from tuning its inherent filtering properties towards a peak sensitivity in the respective frequency range. The cricket *Gryllus bimaculatus* is a simple biological system for which only a narrow range of modulation frequencies is behaviorally relevant. I examined individual neurons in the peripheral and higher auditory system for tuning towards specific temporal parameters and modulation frequencies. To this end, I combined extracellular electrophysiology with different stimulation paradigms involving amplitude-modulated sounds. Analysis of the experimental data revealed that—even in the auditory periphery—some of the examined neurons acted as tuned band-pass filters, yielding highest firing-rates for behaviorally relevant modulation frequencies. Using simple computational models, I demonstrate how common, cell-intrinsic or network-based mechanisms could account for the experimentally observed firing-rate resonances. These mechanisms include subthreshold resonances, spike-triggered adaptation, as well as the interplay of excitation and inhibition. I present how a serial combination of such elementary filters could explain the strong selectivity evident in the cricket's behavior—without the need for a dedicated filter element. Pervasive neuronal mechanisms could therefore constitute an efficient, distributed frequency filter in a highly specialized, size-constrained neuronal system.

Zirpy! Es tut mir leid, wir können jetzt nicht mehr zurück. Ich habe dich schon zu lange festgehalten. Lebe wohl, mein Freund!

—Jan Jannowitz

Contents

Illustrations

Figures

Tables

Abbreviations

AM amplitude modulation
AN ascending neuron
AP action potential
CF carrier frequency
DC duty cycle
DFT discrete Fourier transform
DWT discrete wavelet transform
FSL first-spike latency
GUI guided user interface
HFU high-frequency unit
ISI interspike interval
ISR instantaneous spike rate
KDE kernel density estimation
LFU low-frequency unit
LN linear-nonlinear
MTF modulation transfer function
ON omega neuron
PCA principal component analysis
PDF probability density function
PSTH peristimulus time histogram
RC resistance, capacitance
RLC resistance, inductance, capacitance
rMTF rate modulation transfer function
SAM sinusoidal amplitude modulation
SD standard deviation
SEM standard error of the mean
SFAM swept-frequency amplitude modulation
SPC superparamagnetic clustering
SPL sound pressure level
STFT short-time Fourier transform
tMTF temporal modulation transfer function
VS vector strength
ZAP impedance amplitude profile

1 Introduction

Tuned filters play a vital role in communication: In order to accurately receive a signal through a noisy transmission channel, the receiving side benefits from narrowing and centering perception to the spectral characteristics of the signal (Shannon, 1948). This also applies to neuronal communication (Borst and Theunissen, 1999); strictly speaking, neuronal pathways can be regarded as collections of interconnected, tuned filters. Obvious examples are linked to sensory systems, where highly convergent signal pathways economize the broad information from the outside world into a manageable stream of information (Barlow, 1961). Here, tuned resonances equip neurons with the ability to resolve and efficiently encode spectral components of a stimulus—take, for instance, the Gabor filters proposed for the mammalian auditory system (Smith and Lewicki, 2006) or the electrical tuning of hair cells in lower vertebrates (Fettiplace, 1987). Given their sequential connectivity, the filtering characteristics of individual neurons accumulate, resulting in a gradual increase in selectivity and functional specialization along a given neuronal pathway. This is best illustrated by the mammalian visual system, which ranges from the contrast sensitivity of retinal ganglion cells (Kuffler, 1953), via the detection of visual primitives in striate cortex (Hubel and Wiesel, 1962, 1968), to the invariant object representation found in higher visual areas of the temporal lobe (Gross et al., 1969; Perrett et al., 1982; Quiroga et al., 2005).

Neuronal filtering could play a decisive role in specialized sensory systems. For sensory systems that are dedicated to detecting a narrow range of stereotyped signals, one can expect to find various evolutionary optimizations towards receiving these signals in an efficient and reliable way (Cariani, 2001). The spectral tuning of neurons poses an obvious target for such adaptations. Furthermore, filtering cascades that arise from ubiquitous, cellular or simple network level mechanisms could obviate the need for dedicated filtering elements and play an important role in facilitating efficient computation in particularly small or size-constrained systems. To follow up on these arguments, I investigated the presence of firing-rate resonances in a well-described, small and highly specialized sensory network—the auditory system of the cricket *Gryllus bimaculatus*.

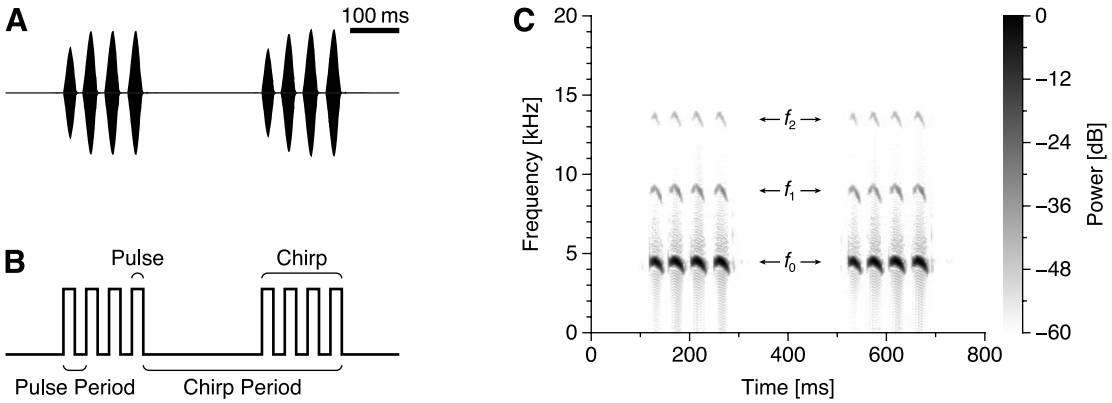

Figure 1.1 The calling song of male crickets (*G. bimaculatus*). **A:** Waveform. **B:** Temporal parameters. **C:** Spectrogram, visualizing the calling song's fundamental frequency ($f_0 \approx 4.5\,\text{kHz}$) and two harmonics ($f_1$ and f_2). Recording courtesy Raimund Specht, Avisoft Bioacoustics.

The cricket as a model organism. The calling songs of male crickets consist of an amplitude modulated, almost pure-tone carrier, structured into a stereotyped, species-specific sequence of short sound pulses (Bennet-Clark, 1989). In case of *G. bimaculatus*, the calling song has a carrier frequency of ~4.5 kHz and is characterized by a pulse period of ~40 ms, with pulses grouped into chirps at a period of ~400 ms (fig. 1.1; Doherty, 1985; Grobe et al., 2012). Female crickets evaluate the temporal features of the male song (fig. 1.1*B*) on the levels of both pulses and chirps (Grobe et al., 2012; Meckenhäuser et al., 2013). In doing so, they are able to recognize and selectively track the rhythmic calling songs of conspecific males in a behavior known as phonotaxis (Regen, 1913; Popov et al., 1976). The female cricket's mate choice yields an effective behavioral barrier to hybridization between closely related species (Gray and Cade, 2000; Wilkins et al., 2013). In addition to its processing of intraspecific songs, the cricket's auditory system is also adapted for perceiving higher-frequency sounds (Suga, 1968; Wohlers and Huber, 1982): The ultrasonic cries of predatory bats trigger *negative* phonotaxis—that is, evasive behavior (Popov and Shuvalov, 1977; Moiseff et al., 1978).

The phonotactic preferences of female crickets can be assessed in behavioral experiments: To do so, the cricket is placed on a walking compensator (Kramer, 1976; Weber et al., 1981) and exposed to synthetic songs with varying spectrotemporal features. One can then assess the directness of the cricket's walking in relation to the stimulus source as an indicator for the animal's phonotactic preference. Two different kinds of periodic waveforms are commonly used as envelope functions for artificial calling songs: sine waves and square waves. When exposed to stimuli with a sinusoidal amplitude modulation (SAM), females of *G. bimaculatus* show a clear behavioral preference towards modulation frequencies

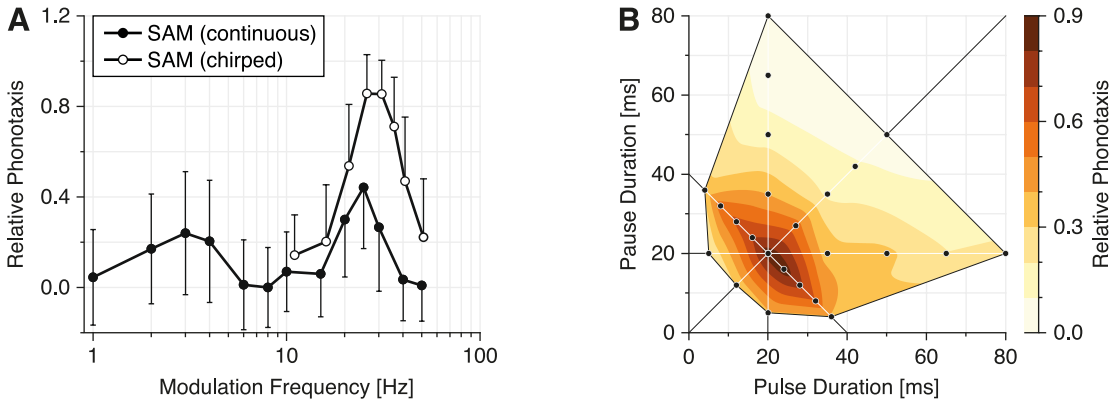

Figure 1.2 Phonotactic preferences of females crickets (*G. bimaculatus*). **A:** Phonotactic responses to 4.5 kHz tones with a sinusoidal amplitude modulation (SAM). Using continuous SAM stimuli (closed circles), two response peaks are apparent: one at 3 Hz and one at 25 Hz. These frequencies correspond to the chirp and pulse rates of the male cricket's calling song. The strongest phonotactic responses are obtained, if the two frequencies are combined—that is, for 25 Hz SAM stimuli grouped in 3 Hz chirps (open circles). Errorbars: SD. Modified from Hennig, 2009, fig. 2. **B:** Phonotactic responses to square-wave modulated tones of 4.5 kHz carrier frequency, presented in chirps (3 Hz). The paradigm enables for stimuli with varying duty cycles. Measured data points are indicated by filled circles. Data extracted from Hennig, 2009, fig. 7*b–e* and plotted according to section 3.2.3.

of ~3 Hz and ~25 Hz (fig. 1.2*A*), corresponding to the chirp and pulse rates of the male cricket's calling song. Square-wave modulated stimuli yield comparable results (Hennig, 2009), with highest phonotactic preferences towards artificial songs with a ~40 ms pulse period (fig. 1.2*B*). As the pulse and pause durations of square waves can be controlled independently from one another, a larger stimulus space can be encompassed than with symmetrical SAM stimuli.

What are the neuronal correlates of phonotaxis? In the cricket's brain, several higher-order neurons have previously been found to respond selectively to acoustic stimuli that match the temporal features of the cricket's song (Schildberger, 1984; Zorović and Hedwig, 2011; Kostarakos and Hedwig, 2012). The nature of these filters, however, is still debated: concepts include template matching (Hoy, 1978; Hennig, 2003), delay lines (Reiss, 1962; Weber and Thorson, 1989), subthreshold current oscillations (Eilts-Grimm and Wiese, 1984; Bush and Schul, 2006; Webb et al., 2007) and band-pass formation through interaction of low- and high-pass neurons (Schildberger, 1984). Interestingly, the sharpness of tuning in the cricket's brain appears to increase from neuron to neuron in sequence of processing (Schildberger, 1984; Zorović and Hedwig, 2011; Kostarakos and Hedwig, 2012), hinting towards distributed filtering mechanisms. Given the behavioral importance of the rhythmic calling songs and the specialized nature

of the cricket's auditory system, a tuning of peripheral neurons towards relevant frequency ranges may be an beneficial adaptation for this size-constrained network (Tunstall and Pollack, 2005).

The scope of this thesis. Through the lens of cybernetics, an experimental subject can be regarded as a *black box*—a system whose inner workings are unknown, but whose *transfer characteristics* can be inferred by relating the system's controllable *input* to its measurable *output* (Wiener, 1961). For instance, one can infer a cricket's phonotactic preferences by relating the parameters of a systematically varying acoustic stimulation to the animal's phonotactic behavior (cf. fig. 1.2). Given the transfer characteristics of a system, one can then try to draw conclusions as to possible implementations. Eventually, one might decide to have a closer look at the system and "open" the black box. Certainly, one will then face more black boxes—the components of the initial system—which can be characterized accordingly[1].

In the course of this thesis I investigate the neuronal correlates of phonotaxis, with particular regard to the filtering properties of the cricket's peripheral auditory system. To this end, I combined different stimulation paradigms involving amplitude-modulated sounds with the extracellular recording of neuronal activity in the cricket's prothoracic and higher auditory system. The experimental black box thus extended from the mechanoreception in the cricket's ears to the neuronal activity at the respective recording site. By relating the parameters of stimulation with the firing rate of selected neurons, I was able to assess the neurons' transfer characteristics—that is, their tuning towards specific stimulus parameters as conveyed by firing-rate resonances.

The experimental approach revealed that—even in the auditory periphery—some of the examined neurons acted as tuned filters, yielding highest firing-rates in response to behaviorally relevant modulation frequencies (chapters 3 and 4). Based on these findings, I inferred feasible filter implementations by means of simple computational models. I thereby demonstrate how ubiquitous, cell-intrinsic or network-based mechanisms could account for the experimentally observed firing-rate resonances (chapter 5). Finally, I speculate about how a serial combination of such elementary filtering mechanisms could yield the strong selectivity evident in the cricket's behavior *en passant*—that is, without the need for a dedicated filter element. Pervasive neuronal mechanisms could therefore constitute an efficient, tuned filtering cascade in a highly specialized, size-constrained neuronal system.

[1] This process continues *ad infinitum*, unless the experimenter loses interest in his subject.

2 General Methods

The experimental methods used in chapters 3 and 4 have a large overlap which is pooled here for the sake of conciseness. Methods specific to the studies are detailed in the respective chapters.

2.1 Animals

All electrophysiological experiments were performed on adult female crickets of the species *Gryllus bimaculatus* De Geer. Animals were reared in-house, kept at room temperature and subjected to a natural light-dark cycle (geographic latitude: 52°31′50″N). They were fed on water and a mixture of rolled oats and bird food (Trockenmischung fein, Aleckwa, Limburgerhof, Germany). Animals qualified for experiments, if they were between two and two-and-a-half months old and physically intact. Before preparation, special care was taken in scrutinizing the integrity of the animal's tympana.

2.2 Preparation

2.2.1 Preparation of the Neck Connectives

The antennae, both pairs of wings as well as the meso- and metathoracic legs were cut off and the animal was dorsally attached to a metal animal holder using beeswax. The head was carefully tilted backwards, exposing the cervix and putting the neck connectives under light tension. To arrange for a steady and largely natural posture of the animal's prothoracic legs, its coxae and tarsi were attached to a supporting steel wire. Meanwhile, care was taken not to constrict the tympana with wax.

To eliminate mechanical interferences caused by intestinal peristalsis, maxillae and labium were removed, the oesophagus was severed and the animal's entire gut was extracted through an abdominal section. The resulting lesion was

thoroughly flushed with insect ringer (Pearson and Robertson, 1981) to avoid tissue damage via digestive enzymes. Neuronal activity extraneous to auditory processing was reduced by removing the meso- and the metathoracic ganglia and cutting the neck connectives close to the suboesophageal ganglion.

A ventral window was cut into the cervix and the tracheae, neck muscles and surplus fat tissue were removed, exposing the neck connectives. After lifting one of the connectives onto a bipolar hook electrode, the cavity was carefully dried with tissue paper and finally sealed with a viscous mixture of petroleum jelly and mineral oil to provide electrical insulation and prevent the preparation from drying out.

2.2.2 Preparation of the Prothoracic Ganglion

To expose the prothoracic ganglion, a preparation similar to the one described in the previous section was carried out: After cutting the antennae and the meso- and metathoracic appendages, the animal was dorsally attached to a metal platform with its prothoracic legs fixed in a natural posture. Maxillae, labium, gut and the metathoracic ganglion were removed and the neck connectives were cut. The mesothoracic ganglion was left in place to mechanically stabilize the prothoracic ganglion via the connectives.

A window was cut into the prosternum. The cavity was carefully cleaned from surplus fat tissue to expose the prothoracic ganglion. Tracheae were left intact. The prothoracic ganglion was mechanically stabilized on a small metal spatula which also served as an indifferent electrode during recordings. After removing excessive hemolymph with tissue, petroleum jelly was applied to the edges of the opening. Finally, the cavity was filled with mineral oil, providing for electrical insulation, protection against dehydration and a clear view onto the prothoracic ganglion.

2.2.3 Preparation of the Brain

A more complex animal holder had to be devised for extracellular recordings from the brain (fig. 2.1*A*). It featured a platform that was freely moveable around a ball joint, allowing for greater flexibility during the preparation. After cutting off the antennae, both pairs of wings and the meso- and metathoracic legs, the cricket was ventrally fixed to the platform with bees wax. The prothoracic legs were attached to a supporting steel wire in a natural posture. The head was tilted slightly backwards to expose frons and clypeus. Postocciput and pronotum were conjoined with wax to strengthen the rigidness of the head posture.

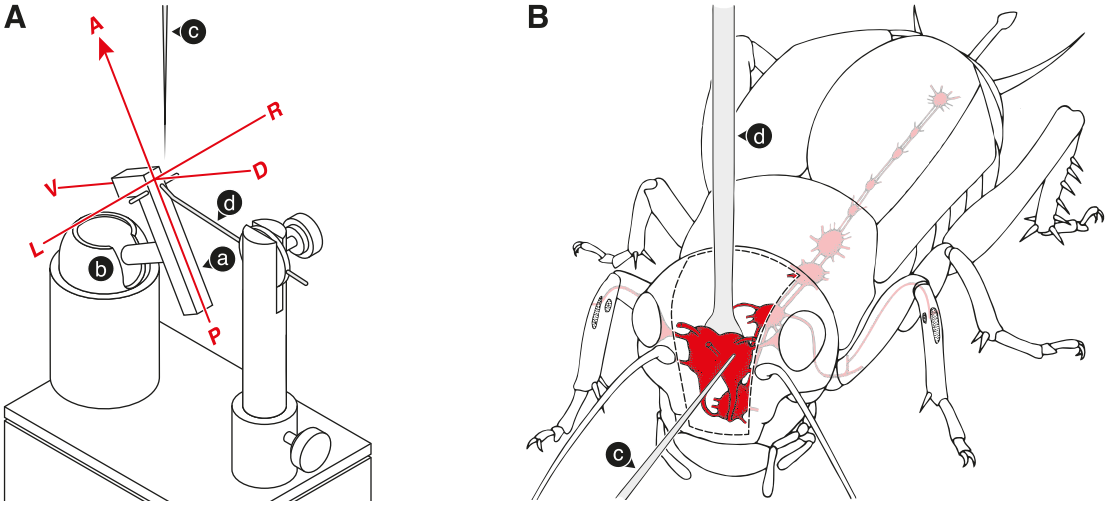

Figure 2.1 Experimental setup and animal preparation for brain recordings. **A:** Animal holder. The cricket was fixed ventrally to a platform (a) using bees wax. The platform could be rotated by means of a ball joint (b). During experiments, the animal was positioned with its anterior pointing upwards towards the recording electrode (c). The latter was referenced to a metal spatula (d). Body axes are indicated in red. **B:** To access the cricket's nervous system (red), a window (dashed line) was cut into the cuticula of the animal's head. A metal spatula (d) was used to mechanically support the brain and to provide a potential reference for the recording electrode (c). Modified from Huber and Thorson (1985).

The head capsule was then carefully opened with a broken razor blade. To avoid damaging the brain during removal of the sclerites, special care was taken in cutting the ocellar nerves. The resulting window ranged from the posterior margin of the vertex to the clypeus and was laterally delimited by the compound eyes (fig. 2.1*B*). The bases of the antennae were removed. Using a piece of tissue, the brain was freed from surplus fat; the tracheae were left intact.

By tilting the platform, the animal's anterior end was oriented upwards toward the recording electrode (cf. fig. 2.1*A*). A metal spatula was inserted under the protocerebrum and carefully lifted upwards to expose the brain (fig. 2.1*B*). It also served as an indifferent electrode during recordings. Petroleum jelly was applied to the edges of the opening and the cavity was filled with insect ringer, providing a clear view onto the brain.

2.3 Electrophysiology

Signals from AN1 and AN2 were recorded differentially (EXT-10C, npi electronics, Tamm, Germany) from one of the neck connectives using a pair of hook electrodes. The latter were manually constructed from 100 µm tungsten wire

with a galvanically tapered tip. A silver wire in the animal's abdomen served as an indifferent electrode.

Units in the prothoracic ganglion and the cricket's brain were recorded with a 500 kΩ extracellular tungsten electrode (World Precision Instruments, Sarasota, FL, USA). A stabilizing metal spatula served as an indifferent electrode. Recordings in the prothoracic ganglion targeted the anterior processes of ON1 close to the ganglionic midline (cf. Wohlers and Huber, 1982, fig. 2). In the cricket's brain, recordings targeted auditory units in the ventral protocerebrum, next to the optical nerve (cf. Kostarakos and Hedwig, 2012, fig. 1).

Voltage signals were band-pass filtered between 300 Hz and 3 kHz (DPA-2FX, npi electronics), digitized at a sampling rate of 20 kHz (PCI-6229, National Instruments, Austin, TX, USA) and recorded to the hard disk of a personal computer using custom software (LabVIEW, National Instruments). Recordings were performed at a room temperature of 19 °C to 22 °C, unless stated otherwise.

2.4 Acoustic Stimulation

All experiments were based on free-field stimulation with amplitude modulated (AM) pure tones. Throughout the cricket's auditory system one can observe a dichotomy between pathways that are sensitive to low carrier frequencies (CFs) and those that are sensitive to high carrier frequencies (Popov, Shuvalov and Markovich, 1976; Boyan and Williams, 1982; Schildberger, 1984). In order to adequately stimulate both pathways, carrier frequencies of either 4.5 kHz or 16 kHz were used, coinciding with the respective characteristic frequencies of the ascending neurons AN1 and AN2 (cf. Schildberger, 1984, fig. 2).

Stimuli were designed digitally (MATLAB, MathWorks, Natick, MA, USA) at a resolution of 100 kS/s. Custom LabVIEW software (National Instruments) was used to play back the stimuli during experiments. After digital-to-analog conversion (PCI-6229, National Instruments), stimulus intensity was adjusted to the desired sound pressure level (SPL) with an attenuator (ATN-01M, npi electronics). The signal was amplified with a power amplifier (Raveland XA-600, Blaupunkt, Hildesheim, Germany) and presented via one of two air motion transformers (X-ART, ADAM Professional Audio, Berlin, Germany) mounted on either side of the animal.

The stimulation system was routinely calibrated to dB re 2 µPa (SPL) with a ½ inch condenser microphone (Type 4133, Brüel & Kjær, Nærum, Denmark) and a precision sound level meter (Type 2231, Brüel & Kjær). To minimize external noise and acoustic reflections, the experimental setup was lined with absorption panels (aixFOAM, Eschweiler, Germany).

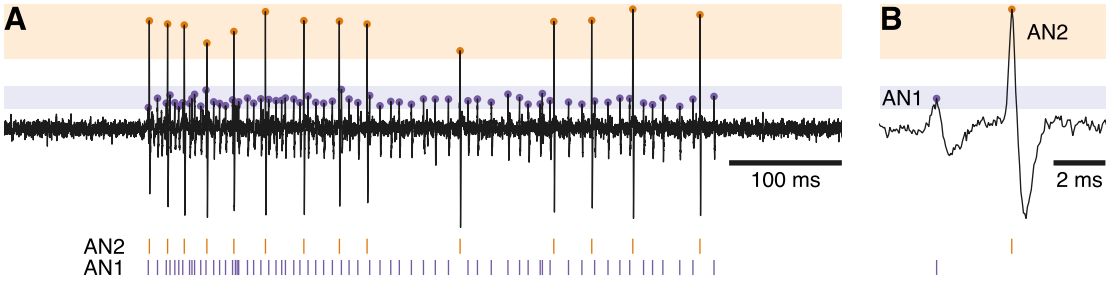

Figure 2.2 Amplitude-based spike sorting. **A:** Extracellular potential recorded from a cricket's neck connective during stimulation with a 4.5 kHz tone of 500 ms duration and 80 dB SPL. Spikes from AN1 and AN2 can be distinguished by their peak amplitude alone. During spike sorting, detection windows (highlighted areas) are defined for each cell type. Signal peaks that fall in between a detection window's lower and upper amplitude bounds are counted as APs of the respective unit and their timing relative to stimulus onset is registered. Ultimately, the continuous extracellular potential is converted to discrete timestamps of spike events. **B:** Detail illustrating the spike shapes of AN1 and AN2.

2.5 Spike Sorting

The electrophysiological experiments performed were based on the extracellular recording of neuronal activity. The extracellular potential is composed of the transmembrane currents of *several* neurons in the vicinity of the recording electrode. A neuron's contribution to this potential is influenced by its morphology, its distance and orientation towards the electrode, the filtering properties of the surrounding tissue and the characteristics of the electrode (Gold et al., 2006; Pettersen and Einevoll, 2008). Assuming that each neuron's stereotyped action potentials (APs) leave characteristically shaped spikes in the extracellular potential, one can classify these spikes into distinct groups or *units* of similar shape. Ideally, spikes of a unit originate from a single neuron and can thus be used to infer the points in time, when the latter fires an AP. This procedure is known as spike sorting.

Spike sorting involves three fundamental steps: (1) detection of spikes in the raw extracellular signal; (2) selection of distinctive spike features; and (3) clustering of the spikes by these features (Quiroga et al., 2004). In the course of this thesis, two different strategies of spike sorting were pursued, differing in both the choice of discriminative features and clustering methods.

2.5.1 Amplitude-based Spike Sorting

In differential recordings obtained from the cricket's neck connectives, spikes of AN1 and AN2 can be distinguished solely by their peak amplitudes (Hennig,

1988), rendering the application of computationally more complex approaches unnecessary. Amplitude-based spike sorting was realized with a custom, GUI based software devised in MATLAB (MathWorks). After loading the raw voltage recording from an experiment, the user could manually define lower and upper amplitude bounds for each cell type (fig. 2.2). For a signal segment to be regarded as a spike, it had to cross the lower amplitude bound during rise, peak below the upper bound and cross the lower bound again during decay. The peak time relative to the onset of the stimulus was then registered as a discrete firing event of the respective unit and saved to a data structure for further analyses.

Spikes of AN1 in some cases had a particularly low amplitude barely above the recording's noise background (Faulkes and Pollack, 2000). In these cases, one either had to trade false-positive spikes off against missed spikes (cf. fig. 4.3) or discard information about AN1 altogether.

2.5.2 Wavelet-based Spike Sorting

In recordings from the ganglia, APs from different neurons could often not be separated by their peak amplitude alone. For this reason, a more elaborate method of spike sorting was adapted from Quiroga et al. (2004). It involved feature extraction using both discrete wavelet transform (DWT) and principal component analysis (PCA), followed by a classification either by superparamagnetic clustering (SPC; Blatt et al., 1996) or by the *k*-means algorithm (MacQueen, 1967). Most of the automated features presented in Quiroga et al. (2004) were replaced with manual alternatives, resulting in a fully supervised approach to spike sorting.

Spike Detection and Extraction. Spikes in the extracellular potential were detected by means of manual amplitude thresholding (fig. 2.3*A*). Subsequently, short segments of their waveform were extracted from the recordings (fig. 2.3*B*).

The segments had to be a multiple of 8 samples in length to meet the requirements of the DWT; in most cases, either 32 or 40 samples were used, corresponding to durations of 1.6 ms or 2 ms. To avoid misalignment caused by aliasing, spike shapes were upsampled by a factor of 5 using cubic splines, aligned by their maxima and downsampled back to their original sampling rate. To allow for changing signal characteristics during the long recording sessions, spikes were processed in separate chunks of 5000 to 10 000 consecutive spikes. Stimulus intensities above ~86 dB SPL led to crosstalk between speaker and electrode; corresponding trials were discarded, as they contained distorted spikes with negative impact on the performance of the clustering algorithms.

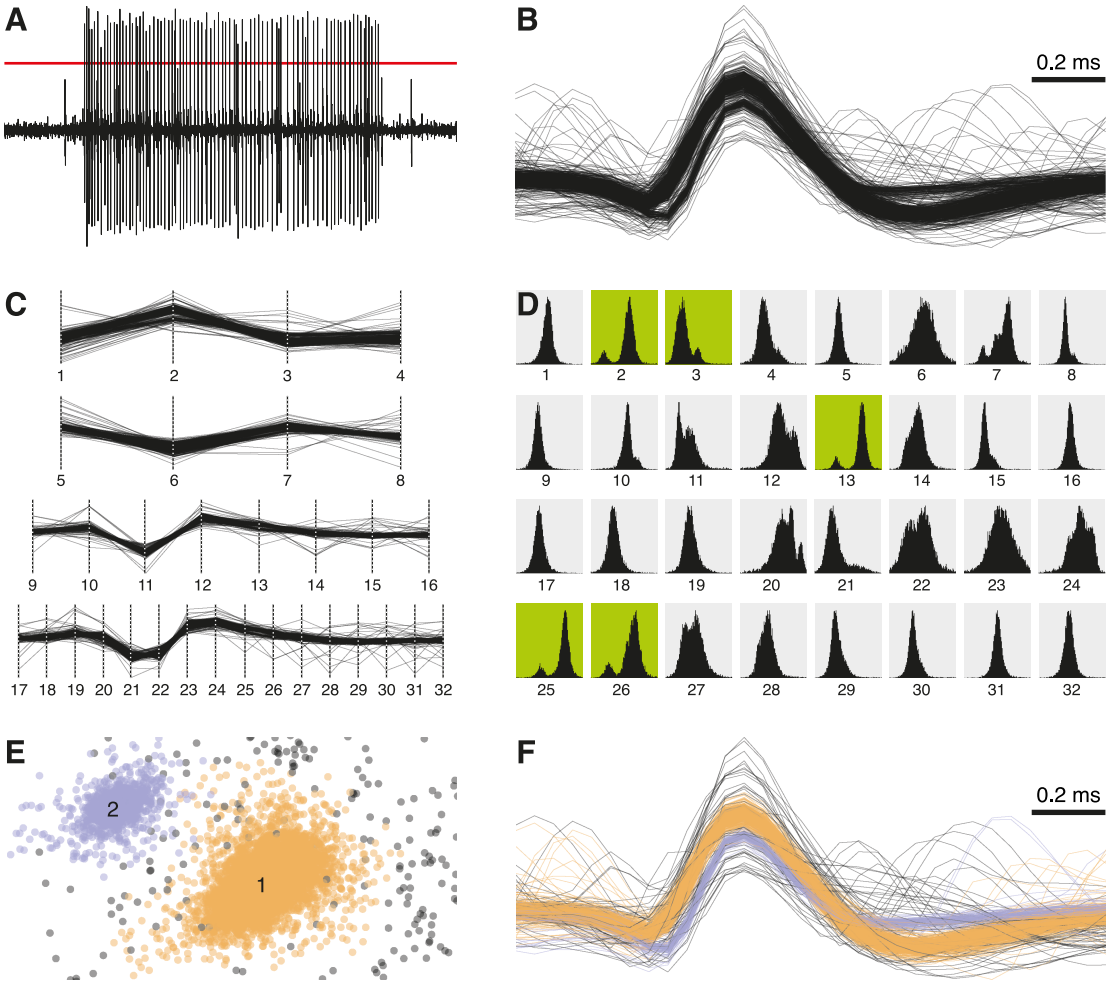

Figure 2.3 Wavelet-based spike sorting. **A:** Spikes that exceeded a manually set threshold (red) were selected for further analysis. Depicted here is a recording from the cricket's brain during stimulation with a 4.5 kHz tone of 500 ms duration and 80 dB SPL. **B:** Segments of the spikes' shapes were extracted from the raw data, interpolated and aligned by their maxima. **C:** Features were extracted by means of a DWT that separated spike characteristics occurring on different time scales. Numbers indicate the individual DWT coefficients. **D:** DWT coefficients that best separated the spike classes exhibited clear bi- or multimodal distributions and were manually selected for clustering (green). **E:** Coefficients 2 (abscissa) and 3 (ordinate) of the data depicted above. The SPC algorithm identified two units (orange and blue). Outliers are indicated in black. **F:** Waveforms of the two units (orange and blue) and outliers (black).

Feature Extraction. Features were extracted by means of a three-level Haar DWT (Haar, 1910) that produced a multiresolution bandpass representation of the original waveforms—that is, it separated the spikes' temporal features by the time scales they occured on (fig. 2.3*C*). The procedure yielded as many candidate coefficients for clustering as there were samples in the waveform segments. Additional features were gathered by computing the first two principle components of the spike shapes. The coefficients that best separated the spike classes—by definition—exhibited multimodal distributions and were manually selected for clustering (fig. 2.3*D*).

Clustering. Clustering of the features (fig. 2.3*E* and *F*) relied on the SPC algorithm (Blatt et al., 1996) or, alternatively, on the *k*-means algorithm (MacQueen, 1967). The choice of algorithm depended on the complexity of the individual clustering problem: If clusters were of similar size and had convex, hyperspherical shapes, *k*-means clustering performed sufficiently accurate, faster and more stable than SPC. Given more complexly shaped clusters, however, SPC was chosen, as it produced fewer evident misclassifications and outliers.

A pre-compiled C++ version of the SPC algorithm was obtained as part of the `Wave_clus` toolbox by Quiroga et al. (2004). MATLAB (MathWorks) calls to the SPC algorithm were loosely based on the implementation in `Wave_clus`. In contrast to the latter, however, the user had to manually define the number of units in the data; if the algorithm returned additional clusters that exceeded this number, they were discarded as outliers.

For *K*-means clustering, the implementation provided by MATLAB (MathWorks) was used. Clusters were normalized to zero mean and unit-variance; elements that exceeded an individually set Euclidian distance to the cluster centers were discarded as outliers.

Distributions of interspike intervals (ISIs) were used to assess the success of the spike sorting procedure, with low ISIs indicating incorrect classifications. Chunks of data were merged; each spike's timing relative to stimulus onset was registered as a discrete firing event of the respective unit and saved to a data structure for further analyses.

2.6 Data Analysis

2.6.1 Cell identification

Lacking the means for morphological reconstructions, classification of recorded units was based on their physiological properties. Ascending neurons—by

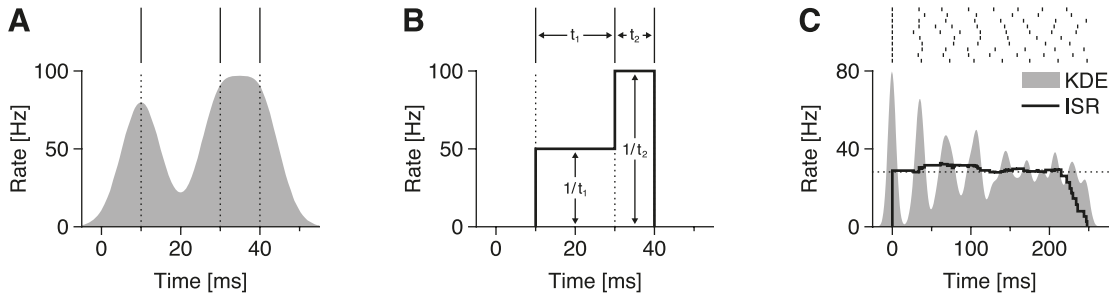

Figure 2.4 Estimation of Firing Rates. **A:** Kernel density estimation (KDE). Spike trains are convolved with a Gaussian kernel function (width $\sigma = 5$ ms). **B:** Instantaneous spike rate (ISR). Consecutive spikes define the edges of histogram bars; their height is given by the reciprocal of the respective ISIs. **C:** To illustrate the characteristics of KDE and ISR, spike trains were generated by means of a gamma processes (cf. section 4.2.5). Spike events occurred at an average rate of 30 Hz. While the 10 trials started off identically, they gradually desynchronized. The KDE (Gaussian kernel, $\sigma = 5$ ms) reflected inter-trial synchronization and exhibited high rates for spikes occurring at similar times across trials. The ISR, however, closely traced the mean rate at all times.

definition—could be directly targeted by recording from the crickets' neck connectives. In this recording configuration, AN2 can be distinguished from AN1 by its sensitivity to high carrier frequencies and its larger AP amplitude (Hennig, 1988). The local prothoracic unit ON1 has a characteristically broad spectral tuning. It was identified by its greater sensitivity, but longer response latency, to stimulation at 4.5 kHz compared to 16 kHz (for *Teleogryllus oceanicus*: Faulkes and Pollack, 2000; Sabourin et al., 2008). Neurons recorded in the cricket's brain were grouped by a broad set of physiological properties, including spectral sensitivity, response latencies and temporal tuning. For details, refer to chapter 3.

For AN1 and AN2, the terms contralateral and ipsilateral are used with reference to their ascending axon. For ON1 and all units recorded from the cricket's brain, the terms are used with reference to the stimulus orientation that led to the stronger firing-rate response.

2.6.2 Estimation of Firing Rates

To estimate the firing rates of recorded neurons, both kernel density estimation (KDE; Parzen, 1962; Rosenblatt, 1956) and instantaneous spike rates (ISR; Bessou et al., 1968) were utilized. The measures represent different aspects of multi-trial recordings.

KDE represents both rate and timing of APs by estimating their temporal distribution. To construct the KDE of a spike train, the latter was convolved with a Gaussian kernel function (fig. 2.4*A*). The Gaussian's width σ controlled the

smoothness of the KDE and was manually set on an individual basis. In order to obtain correct firing rate estimates, the area of the kernel function must equal 1. KDE is closely related to the peristimulus time histogram (PSTH; Gerstein and Kiang, 1960). Unlike the latter, KDE is not prone to aliasing and more accurately reflects the underlying distribution of APs (Nawrot et al., 1999). Because its calculation is based on spike timing, the KDE also contains information about inter-trial variability and stimulus locking (fig. 2.4*C*).

The ISR represents firing rates on the basis of ISIs: Consecutive spikes define the edges of histogram bars; their height is given by the reciprocal of the respective ISIs (fig. 2.4*B*). The ISR can be averaged across trials, resulting in an accurate estimation of firing rates. Because the ISR builds on ISIs rather than AP timing, it is not susceptible to the effects of inter-trial variability (fig. 2.4*C*).

2.6.3 Latency Correction

The time that passes between stimulation of a receptor and response of a particular neuron downstream of this receptor depends on several parameters: Stimulus quality, signal transduction, intra- and intercellular signal transmission and integration. When comparing responses of *different* neurons to a particular external stimulus, one usually has to correct for latency differences.

Latencies were assessed as the time interval between onset of a stimulus and occurrence of the first stimulus-evoked AP, the so-called first-spike latency (FSL; cf. Heil, 2004). The fact that many neurons are spontaneously active constitutes a nontrivial problem in determining the FSL: It is impossible to unambiguously identify individual APs as stimulus-evoked or spontaneous by looking at their timing alone. To address this issue, the FSL was deduced from the stimulus-evoked increase in AP *rate*: First, the spontaneous firing-rate was determined in the 200 ms immediately prior to the stimulus onset and averaged across trials. A threshold was set three standard deviations (or at least 40 Hz) above this baseline. The FSL of a single trial was then given by the time interval between onset of the stimulus and the point at which the ISR first crossed this threshold, indicating a stimulus-related deviation from the spontaneous rate.

For a given neuron and recording session, FSLs were determined for all those trials, whose stimuli featured a sudden, salient onset (i.e., a square envelope). Response latencies to stimuli with identical qualities (sound intensity, carrier frequency and laterality) were pooled by calculating their median. Timestamps of all APs were corrected for latency by subtracting the FSL appropriate for the respective stimulus qualities.

3 Stages of Auditory Processing

3.1 Introduction

The cricket is a classic model organisms for studying the processing of simple, rhythmic sounds with a strong behavioral relevance. With the advent of electrophysiology, several studies have concentrated on the cricket's auditory system, widening our understanding of the neuronal processing of temporally structured signals (Huber et al., 1989). While many working principles of the cricket's auditory system have previously been unveiled, we still lack a profound understanding of the exact mechanisms that underly the recognition of intraspecific signals.

The prevailing idea is that the female cricket exploits a central "recognizer" to identify the temporal features of the calling song, while peripheral elements are merely used for preprocessing and forwarding of the sound information (cf. Horseman and Huber, 1994b, fig. 1). Indeed, *several* higher-order neurons have been found to respond selectively to acoustic stimuli that match the temporal features of the cricket's song (Schildberger, 1984; Zorović and Hedwig, 2011; Kostarakos and Hedwig, 2012). Interestingly, the tuning of these brain neurons appears to be differentially expressed and increase in sequence of processing (Schildberger, 1984; Zorović and Hedwig, 2011). This observation challenges the idea of a dedicated "recognizer" by hinting towards a more distributed processing of temporally structured sound.

This chapter constitutes an comprehensive reevaluation of cell types throughout the cricket's auditory system, encompassing both peripheral and higher-order cell types. Extracellular electrophysiology enabled long-lasting, stable recordings of neuronal activity and allowed for the deployment of an exhaustive stimulation paradigm: Simple, square-wave modulated tones were used to differentiate between physiologically different units and to characterize their temporal processing of sound. Several units were found to preferentially respond to pulse patterns that matched the temporal characteristics of the male cricket's calling song. Interestingly, such behaviorally relevant filtering was not only observed in the brain, but also for units in the auditory periphery.

3.2 Methods

This section only details methods specific to the present study. For a description of the more general methods involved, refer to chapter 2, sections 2.1 to 2.6.

3.2.1 Rate-Intensity Functions

By quantifying an auditory neuron's response to short sound pulses with systematically varying parameters—that is, different carrier frequencies, sound pressure levels and spatial orientations—one can deduce several fundamental, physiological properties: the neuron's dynamic range, its frequency sensitivity, strength of firing-rate adaptation and directional sensitivity. A compact visualization of such data is given by the rate-intensity function—a plot of firing rate versus stimulus intensity.

For stimulation, pure tones of 4.5 kHz or 16 kHz were multiplied with square pulse envelopes of either 500 ms or 1 s duration and presented to either side of the animal. Envelopes were tapered by 1 ms ramps to reduce the emission of spectral splatter by the loudspeakers. Stimulus intensities were systematically varied from either 40 dB to 100 dB SPL in 10 dB increments, or from 48 dB to 104 dB SPL in 8 dB increments. Each stimulus (i.e., a tone with a specific combination of carrier frequency, intensity and direction) was repeated 5, 8 or 10 times.

Two types of rate-intensity functions were measured: *Onset* rate-intensity functions characterize a cell's unadapted response. To this end, the average firing rate was measured within a window of −5 ms to 45 ms relative to the latency-corrected response onset (see section 2.6.3). *Steady-state* rate-intensity functions, on the other hand, characterize a cell's fully adapted response to stimulation. Here, the firing rate was averaged for the period from 300 ms after stimulus onset to stimulus end. Responses across several stimulus repetitions were combined by calculating the median. Individual rate-intensity functions were linearly interpolated (to compensate for different intensity increments) and finally averaged across recordings by cell type.

3.2.2 Latency-Intensity Functions

First-spike latency (FSL; see section 2.6.3) was evaluated as a function of stimulus intensity, building on the same stimulus set used for assessing rate-intensity functions (section 3.2.1). The analogous latency-intensity functions covered stimuli of 4.5 kHz and 16 kHz CF, presented to either side of the animal. Results were linearly interpolated and then averaged across recordings by cell type.

To facilitate a statistical comparison between response latencies of different cell types, FSLs for a subset of stimulus qualities were examined in greater detail. This subset comprised 80 dB SPL stimuli, presented at each cell type's preferred carrier frequency and lateral orientation. The significance of latency differences was verified with a Wilcoxon rank sum test. For the broadly tuned ON1, FSLs at different CFs were compared with a Wilcoxon signed rank test.

Lacking an air-conditioning system, electrophysiological experiments were subject to seasonal variations in ambient temperature. While recordings of AN1, AN2 and ON1 were performed at relatively consistent room temperatures of 19 °C to 22 °C, brain recordings were conducted at a higher and more broadly distributed set of temperatures. Like most physiological processes, transduction and conduction delays depend on temperature (Katz and Miledi, 1965a; Rosenthal and Bezanilla, 2000). For units recorded in the cricket's brain, response latencies were thus assessed as a function of temperature. For this purpose, the ambient temperature within the Faraday cage was measured with a mercury-in-glass thermometer at the beginning of each recording session. Given a sufficiently large sample size, observations were fitted by a simple linear regression model. The significance of the temperature-dependence was assessed by a t-test. Regression models of different units were compared by means of an analysis of covariance (ANCOVA). All statistical tests were performed with MATLAB (MathWorks).

3.2.3 Pulse Response Arrays

The calling song of male crickets corresponds to a pure tone with a characteristic set of temporal features, namely groups of pulses separated by periods of silence (Bennet-Clark, 1989). Female crickets indicate a behavioral preference for a pulse period of ~40 ms (Hennig, 2009), matching the parameters of the male calling song. To investigate how individual auditory neurons process sound information in the temporal domain, animals were stimulated with synthetic calling songs—square-wave modulated tones with systematically varying pulse and pause durations. Pulse and pause durations could be controlled independently from one another, enabling for a stimulation at different duty cycles (DC, ratio of pulse duration and pulse period). Three different sets of stimuli were used:

A. Combinations of pulse and pause durations were covered between 5 ms and 80 ms with a resolution of 5 ms (fig. 3.1*A*). The length of individual pulse patterns was the even multiple of its period closest to 600 ms. Each pulse pattern was preceded by an additional 200 ms pulse, with a 20 ms offset. The purpose of this initial pulse was to ensure a consistent state of adaptation throughout trials.

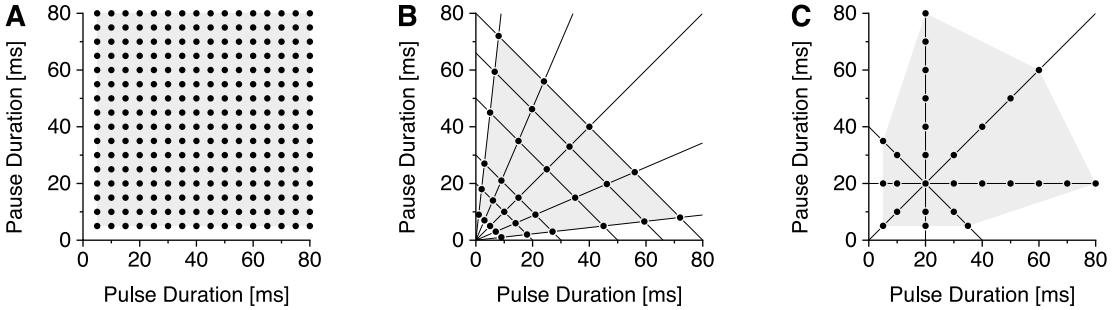

Figure 3.1 Coverage of pulse-pause combinations in three types of stimulus sets. Circles indicate pulse-pause combinations assessed during experiments. The area enclosed by the data points' convex hull (gray) was approximated by natural neighbor interpolation. **A:** Exhaustive coverage of pulse and pause durations with 5 ms resolution. **B:** Smaller set of combinations given by the intersection points of a defined array of periods and duty cycles. **C:** Subset of the combinations in **A** along four cross-sections of the parameter space, intersecting at female crickets' preferred combination of pulse and pause durations.

B. Combinations of pulses and pauses were given by the intersection points of a defined set of pulse periods (10 ms, 20 ms, 30 ms, 50 ms, 66 ms and 80 ms) and pulse duty cycles (0.1, 0.3, 0.5, 0.7 and 0.9) (fig. 3.1*B*). Pulses were presented in two consecutive chirps, with a 500 ms chirp period. The duration of individual chirps was the even multiple of the given pulse period closest to 250 ms. Thus, pulse parameters were varied under behaviorally preferred chirp conditions (cf. Grobe et al., 2012).

C. Stimuli were a subset of set A along four cross-sections of the parameter space (fig. 3.1C). These cross-sections were given by a constant pulse or pause duration (20 ms, respectively), a constant duty cycle (0.5) or a constant period (40 ms). Hence, they intersected at the behaviorally preferred song parameters of *G. bimaculatus* (Hennig, 2009).

In all three cases, stimuli had a carrier frequency of 4.5 kHz and were played from the ipsilateral speaker at 80 dB SPL. They were presented in randomized order, with each stimulus being presented up to 5 (set C) or 10 times (sets A and B), depending on the state of the recording. To avoid spectral splatter, envelopes were tapered by 1 ms (set B) or 2 ms (sets A and C) ramps.

Responses were evaluated by dividing the number of spikes during each pulse pattern by its duration (for stimulus set B only within the second chirp). The resulting firing rates were averaged across trials by calculating their median. To visualize the dependance of firing rates on pulse and pause durations, data were presented as pseudocolor plots. These plots—henceforth referred to as *pulse response arrays*—were interpolated using natural neighbor interpolation (Sibson,

1981). To consolidate results across recordings, pulse response arrays were averaged by cell type. If recordings of a specific cell type comprised stimulations with different sets of pulse patterns (cf. fig. 3.1), only the intersecting area of the respective parameter spaces was averaged. Cross sections of the pulse response arrays illustrate the responses to stimuli with constant pulse or pause durations (20 ms, respectively), constant duty cycle (0.5) and constant period (40 ms).

Responses to stimuli with a constant duty cycle of 0.5 were compared to data from previous studies (Schildberger, 1984, fig. 11; Zorović and Hedwig, 2011, table 1; Kostarakos and Hedwig, 2012, figs. 2*C* and 5). Data was extracted from figures using `GraphClick` (Arizona Software, Neuchâtel, Switzerland). To facilitate a direct comparison, AP counts from Schildberger (1984) were divided by the reported counting window of 300 ms, yielding firing rates. Similarly, AP counts from Kostarakos and Hedwig (2012) were divided by the respective stimulus durations, given by the product of pulse period and pulse count.

3.3 Results

3.3.1 Prothoracic Interneurons

Ascending neuron 1 Rate-intensity functions for AN1 reflected its sensitivity towards low carrier frequencies: at 4.5 kHz, the activity threshold was at 50 dB SPL, with a saturation point at 70 dB to 80 dB SPL (fig. 3.2A_i). Firing rates saturated at approximately 200 Hz. The response to ipsilateral stimulation was stronger that that to contralateral stimulation, as evident from a ~10 dB offset between the respective rate-intensity functions. There was no noteworthy activity at 16 kHz CF, with only a minor increase in firing-rate at 100 dB SPL (fig. 3.2A_{ii}). For both frequency channels, a high noise floor of just below 50 Hz was determined. Latency-intensity functions corroborated AN1's sensitivity towards low carrier frequencies (fig. 3.2$A_{iii,\,iv}$). At 4.5 kHz CF and 80 dB SPL, a median first-spike latency of 20.2 ms was observed (fig. 3.6*A*). Pulse response arrays (fig. 3.2*B*) indicated no notable preference for specific pulse periods: AN1's activity reflected the average power of stimulation, as its firing-rate correlated with the pulse patterns' duty cycle (fig. 3.2C_{ii}).

Ascending neuron 2 For AN2, rate-intensity functions indicated a strong sensitivity towards high carrier frequencies: at 4.5 kHz, the activity threshold was observed at approximately 70 dB SPL; while at 16 kHz, AN2 already commenced firing at 50 dB to 60 dB SPL (fig. 3.2$D_{i,\,ii}$). No clear saturation of firing-rates could be observed within the tested intensity range. Interestingly, in the high frequency

channel, contralateral stimulation was more effective than ipsilateral stimulation. This was also reflected by the latency-intensity functions: high carrier stimuli provoked shorter latencies than low carrier stimuli and an inversion of lateral preference (fig. 3.2$D_{iii,\,iv}$). During stimulation at 16 kHz CF and 80 dB SPL (contralateral), a median first-spike latency of 18.5 ms was observed (fig. 3.6*A*). Pulse response arrays were considerably different from those of AN1 (fig. 3.2*E*). Given the stimulation at 4.5 kHz, AN2's overall activity was low. Most notably, however, AN2 showed a clear deviation from a mere duty cycle dependence: its activity was strongest at a DC of 0.5 and decreased at both lower and higher DC values (fig. 3.2F_{ii}). The most effective period was determined to be approximately 30 ms, with a strong drop-off at lower values and a less pronounced drop-off at higher values (fig. 3.2F_i). Overall, results suggest a preference for pause durations of approximately 20 ms, largely irrespective of the pulse duration (fig. 3.2$F_{iii,\,iv}$).

Omega neuron 1 Rate-intensity functions illustrate ON1's broad sensitivity towards stimuli of both low and high carrier frequencies: at 4.5 kHz, the activity threshold was estimatet at 50 dB SPL; while at 16 kHz, it was at approximately 60 dB SPL (fig. 3.2$G_{i,\,ii}$). In both cases, onset responses reached levels well above 200 Hz. No clear saturation of firing-rates could be observed within the tested intensity range. While the two frequency channels' directional sensitivities were similar (~10 dB offset), the high frequency channel showed a slightly weaker effect of firing-rate adaptation. Both frequency channels manifested low response latencies (fig. 3.2$G_{iii,\,iv}$). At 4.5 kHz CF and 80 dB SPL, a median first-spike latency of 21.7 ms was observed; at 16 kHz CF, it was determined to be significantly lower value of 17.5 ms (fig. 3.6*A*; Wilcoxon signed rank test: $p < 0.001$). The average pulse response array indicated a strong dependence on the stimulus duty cycle (fig. 3.2*H*). This effect, however, saturated for duty cycles above 0.5 (fig. 3.2I_{ii}). Likewise, firing-rates plateaued at pulse durations longer than, and pause durations shorter than 20 ms (fig. 3.2$I_{iii,\,iv}$). A weak preference for periods of 40 ms duration could be inferred (fig. 3.2I_i).

3.3.2 Units Recorded in the Cricket's Brain

Lacking the means for morphological reconstructions, units recorded in the cricket's brain were grouped by physiological properties alone. Units in four of these groups were sensitive to low carrier frequencies (low-frequency units; LFUs), while units in another two groups were primarily sensitive to high carrier frequencies (high-frequency units; HFUs).

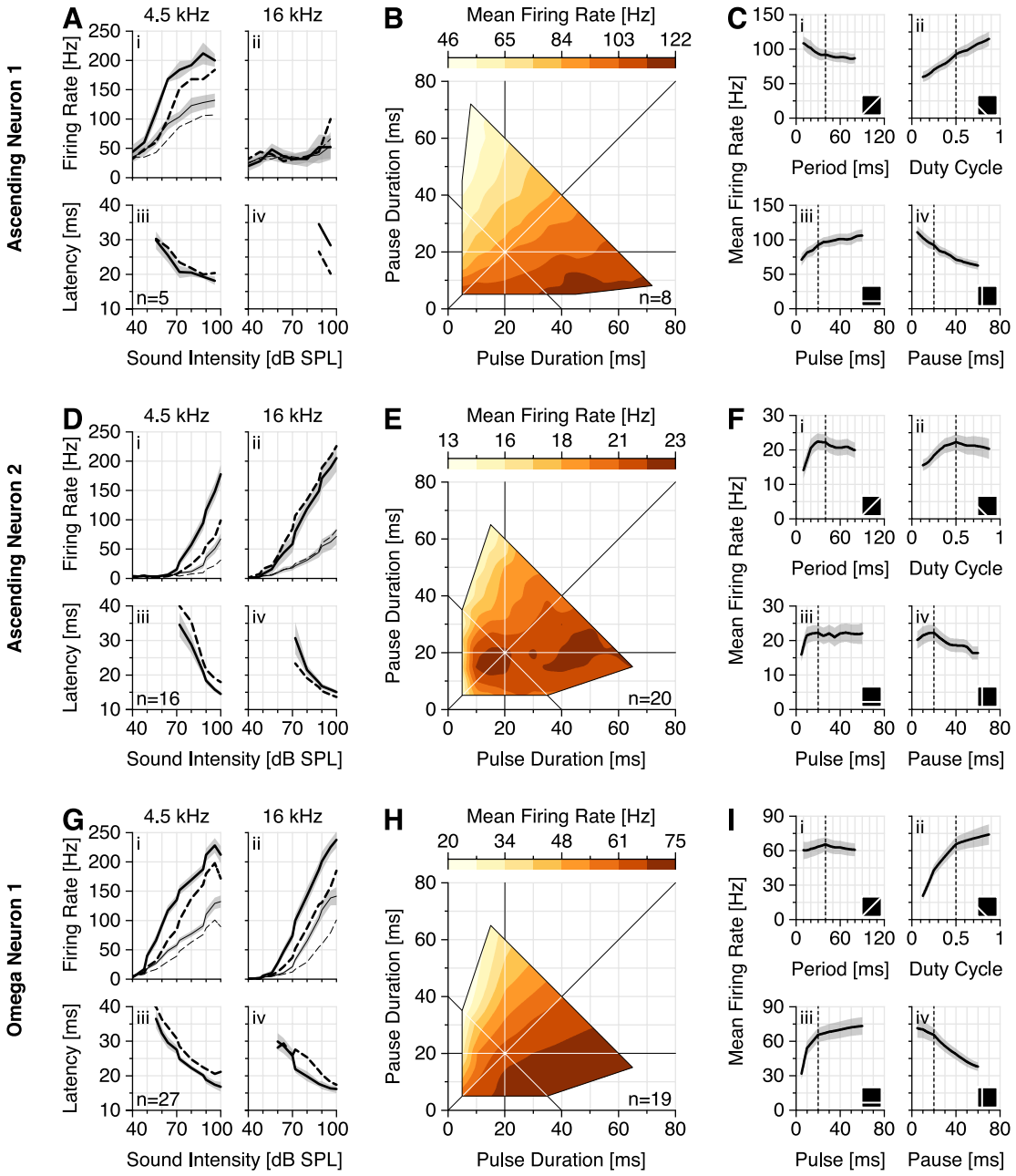

Figure 3.2 Pulse response properties of the prothoracic interneurons AN1, AN2 and ON1. **A, D, G:** Average rate-intensity and latency-intensity functions at 4.5 kHz and 16 kHz CF. Responses to ipsilateral stimulation are indicated by solid lines; responses to contralateral stimulation by dashed lines. Thick lines represent onset responses, whereas thin lines indicate steady-state responses. SEM is indicated in gray (only shown for ipsilateral responses). **B, E, H:** Average pulse response arrays at 4.5 kHz CF. **C, F, I:** Cross sections of pulse response arrays (black), SEM (gray). Pictograms indicate the cross sections' orientation within the parameter space; dashed lines mark the parameters preferred by female crickets.

Low-frequency units 1 and 2 Both LFU1 and LFU2 had physiological properties similar to those of AN1: the two units were very sensitive to stimulation at 4.5 kHz, with a firing threshold of 40 dB SPL or lower (fig. 3.3A_i, D_i). In both cases, onset rate-intensity functions peaked at about 70 dB SPL with a firing rate of approximately 300 Hz. At higher intensities, onset firing rates decreased again. Steady-state rate-intensity functions saturated at about 80 dB SPL, with a maximum firing rate of 250 Hz. The units were more sensitive to ipsilateral than to contralateral stimulation by ~10 dB. The ipsilateral response was leading by about 10 dB SPL (slightly less for LFU1). The most distinct difference between the two units—and the reason why they were classified as such—was given by their responses to stimuli with a high carrier frequency: while LFU1 did not show any noteworthy responses to 16 kHz stimuli (fig. 3.3A_{ii}), LFU2 manifested a considerable activity at intensities above 70 dB SPL, reaching firing rates of 200 Hz or greater (fig. 3.3D_{ii}). This activity, however, only occurred during ipsilateral stimulation. It consistently appeared first in LFU2's steady-state response—only at higher sound pressure levels did 16 kHz stimuli also yield an onset response.

Latency-intensity functions reflected the units' sensitivity towards low carrier frequencies (fig. 3.3$A_{iii,\,iv}, D_{iii,\,iv}$). For stimulation at 4.5 kHz CF and 80 dB SPL, response latencies were additionally evaluated as a function of ambient temperature (fig. 3.6B). Temperature had a significant effect on the FSL of both LFU1 ($\beta = -0.64, R^2 = 0.68, t_8 = -4.1, p = 0.003$) and LFU2 ($\beta = -0.63, R^2 = 0.39, t_{11} = -2.6, p = 0.02$). An ANCOVA revealed that the two regression slopes were not significantly different ($F_{1,19} = 7.4 \times 10^{-4}, p = 0.98$); likewise, there were no significant differences between the Y-intercepts ($F_{1,19} = 0.81, p = 0.38$). Consequently, the two units are probably on the same stage of processing or even variations of the same cell type, albeit with differences in physiological properties. Disregarding the temperature effect, there were no significant differences between the latencies of either LFU1 or LFU2 and AN1 (Wilcoxon rank sum test: $p = 0.31$ and $p = 0.39$, respectively).

The average pulse response arrays of both units (fig. 3.3B, E) indicated a strong dependence on the stimulus duty cycle, but saturated at DC values above 0.5 (fig. 3.3C_{ii}, F_{ii}). Likewise, firing-rates plateaued at pulse durations longer than, and pause durations shorter than, 20 ms (fig. 3.3$C_{iii,\,iv}, F_{iii,\,iv}$). In this regard, the two units behaved similarly to ON1, albeit at higher firing-rates (cf. fig. 3.2H, I).

Low-frequency unit 3 LFU3 was most sensitive to low carrier frequencies: at 4.5 kHz, LFU3's activity threshold was approximately 60 dB SPL, with a saturation point of 80 dB to 90 dB SPL (fig. 3.4A_i). Peak firing rates were registered at approximately 350 Hz. At 16 kHz CF, LFU3 had a relatively high firing thresh-

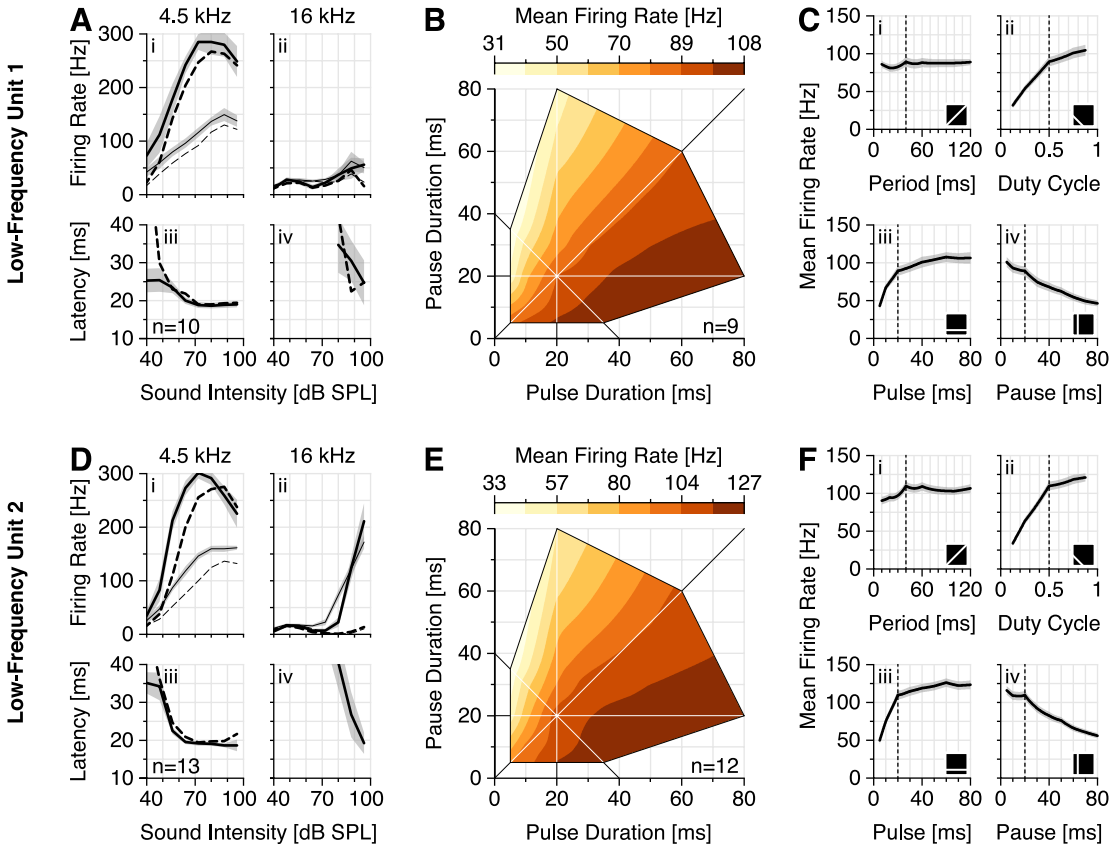

Figure 3.3 Pulse response properties of the low-frequency units LFU1 and LFU2. **A, D:** Average rate-intensity and latency-intensity functions at 4.5 kHz and 16 kHz CF. Responses to ipsilateral stimulation are indicated by solid lines; responses to contralateral stimulation by dashed lines. Thick lines represent the cells' onset response, whereas thin lines indicate their fully adapted steady-state response. The SEM is indicated in gray (only shown for ipsilateral responses). **B, E:** Average pulse response arrays at 4.5 kHz CF. **C, F:** Cross sections of the average pulse response arrays (black) and SEM (gray). Pictograms indicate the orientation of the respective cross section; dashed lines mark the parameters preferred by female crickets.

old of 90 dB SPL (fig. 3.4A_{ii}). The unit did not show any indication of lateral preference. Spontaneous activity was determined at a level of 30 Hz to 40 Hz.

Latency-intensity functions reflected the unit's sensitivity towards low carrier frequencies (fig. 3.4$A_{iii,\,iv}$). Since LFU3 was only recorded once, latency differences could not be confirmed statistically. The FSL observation for stimulation at 4.5 kHz CF and 80 dB SPL, however, was well above the 95 % prediction bands of the regression models for LFU1 and LFU2 (fig. 3.6*B*). While this does not constitute a statistical test, it hints at a higher processing stage and, consequently, a different cellular identity than LFU1 and LFU2.

LFU3 showed a clear preference for the song parameters of *G. bimaculatus* (fig. 3.4*B*). Compared to units with a similar CF preference but lower response latency, LFU3 showed generally lower firing rates and a clear deviation from a mere duty cycle dependence: its activity dropped for, both, low and high DC values, with an optimum at 0.5 (fig. 3.4C_{ii}). The drop-off towards high DC values was considerably more pronounced than that of AN2 (cf. fig. 3.2F_{ii}).

Low-frequency unit 4 The rate-intensity function of LFU4 did not comply with the archetypical sigmoidal shape. At 4.5 kHz CF, the activity threshold was between 70 dB and 80 dB SPL , with an apparent preference for contralateral stimuli (fig. 3.4D_i). Maximum firing rates were observed at a stimulus intensity of 80 dB SPL; at higher values, the unit's response fell off again. At 16 kHz CF, LFU4 had a relatively high firing threshold of approximately 90 dB SPL (fig. 3.4D_{ii}).

Latency-intensity functions reflected the units' sensitivity towards low carrier frequencies (fig. 3.4$A_{iii,\,iv}$). Since LFU4 was only recorded once, latency differences could not be confirmed statistically. The FSL observation for stimulation at 4.5 kHz CF and 80 dB SPL, however, was well above the 95 % prediction bands of the regression models for LFU1 and LFU2 (fig. 3.6*B*), hinting at a higher processing stage and a different cellular identity.

LFU4 showed a sharp tuning towards the song parameters of *G. bimaculatus* (fig. 3.4*E*). LFU4's overall response amplitude was lower than that of LFU3. Its temporal tuning, however, was more pronounced and matched the female preferences (cf. fig. 3.2*F*).

High-frequency units 1 and 2 Both HFU1 and HFU2 had physiological properties similar to those of AN2: the two units were most sensitive to high carrier frequencies, with a firing threshold of 50 dB to 60 dB SPL, reaching peak firing rates between 350 Hz and 400 Hz (fig. 3.5A_{ii}, D_{ii}). Stimulation at 4.5 kHz provoked responses with lower firing-rates, with thresholds between 60 dB and 70 dB SPL (fig. 3.5A_i, D_i). The most distinct difference between the two units—

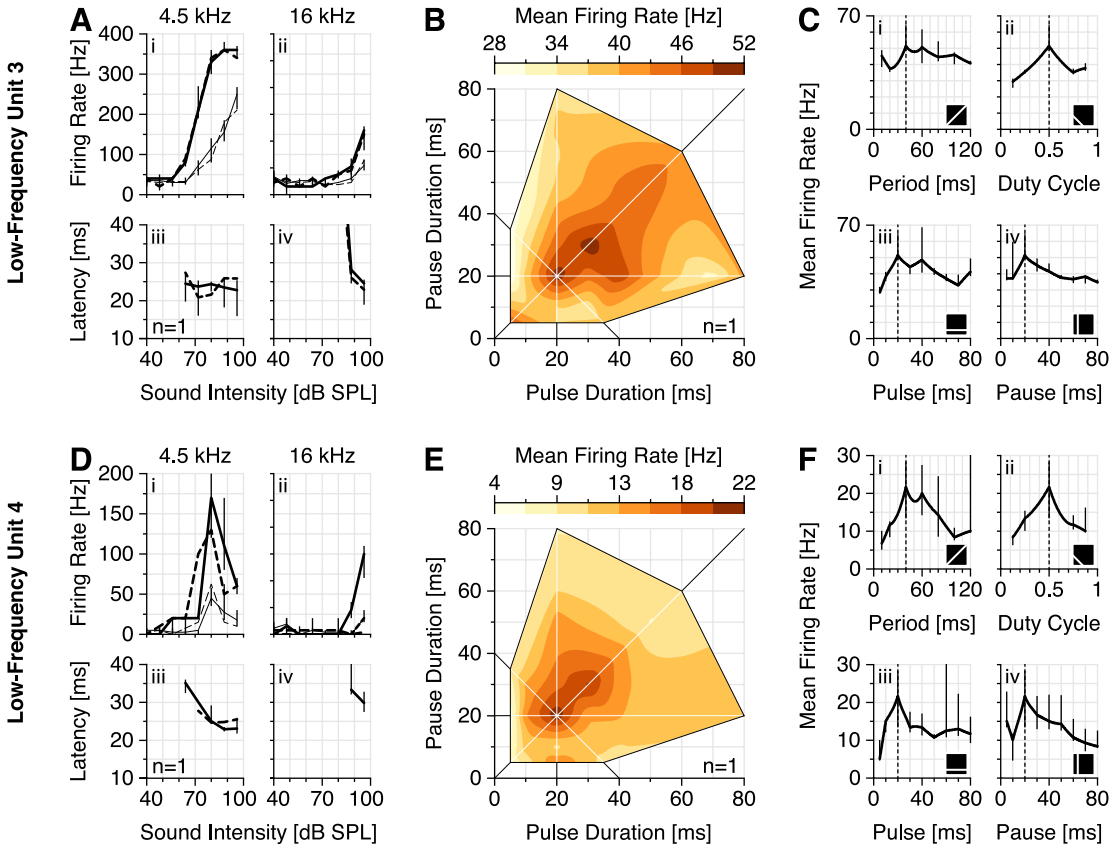

Figure 3.4 Pulse response properties of the low-frequency units LFU3 and LFU4. **A, D:** Rate-intensity and latency-intensity functions at 4.5 kHz and 16 kHz CF. Responses to ipsilateral stimuli are indicated by solid lines; those to contralateral stimuli by dashed lines. Thick lines represent the cells' onset response; thin lines the steady-state response. Error bars indicate the first and third quartile across multiple trials (ipsilateral responses only). **B, E:** Average pulse response arrays at 4.5 kHz CF. **C, F:** Cross sections of the average pulse response arrays. Pictograms indicate the orientation of the respective cross section. Error bars indicate the first and third quartile across multiple trials; dashed lines mark the parameters preferred by female crickets.

analogous to LFU1 and LFU2—lay in the directional sensitivity at high carrier frequencies: HFU1 was more sensitive to ipsilateral stimulation by up to ~10 dB; HFU2, however, showed a distinctively more pronounced directional preference: its onset response to ipsilateral stimuli was approximately twice as strong as the response to contralateral stimuli of identical sound pressure levels. Note that neither of the two units match the characteristics of AN2 in this regard. The steady-state response to contralateral stimuli did not exceed firing-rates of 50 Hz, irrespective of stimulus intensity.

Latency-intensity functions reflected the units' sensitivity towards high carrier frequencies (fig. 3.5$A_{iii,\,iv}$, $D_{iii,\,iv}$). For stimulation at 16 kHz CF and 80 dB SPL, response latencies were additionally evaluated as a function of ambient temperature (fig. 3.6*C*). The response latency of HFU2 had a significant dependence on temperature ($\beta = -0.43$, $R^2 = 0.52$, $t_8 = -3.4$, $p = 0.006$). Due to the small sample-size, data for HFU1 could not be fitted by a regression model. The observed FSLs, however, lay within the 95 % prediction bands of the regression model for HFU2, suggesting that the two units are on the same processing stage or even variations of the same cell type. According to an ANCOVA, the regression slope of HFU2 was neither significantly different from the regression slope of LFU1 ($F_{1,19} = 1.1$, $p = 0.30$), nor from that of LFU2 ($F_{1,22} = 0.62$, $p = 0.44$). The Y-intercepts of HFU2, however, were significantly lower than those of LFU1 and LFU2 ($F_{1,19} = 25$, $p < 0.001$; and $F_{1,22} = 36$, $p < 0.001$ respectively). Disregarding the temperature effect, latencies of HFU2 were significantly shorter than those of AN2 (Wilcoxon rank sum test: $p = 0.021$). Latencies of HFU1, however, were not significantly different from those of AN2 (Wilcoxon rank sum test: $p = 0.22$).

The average pulse response arrays of both units indicated clear preferences for the song parameters of *G. bimaculatus* (fig. 3.5*B, E*). These preferences were apparent in all cross sections of the pulse response arrays (fig. 3.5*C, F*). For HFU1, a secondary preference peak could be detected at a pulse duration of 70 ms and a pause duration of 20 ms (fig. 3.5C_{iii}).

3.4 Discussion

This study represents an extensive characterization of the cricket's peripheral and higher-level auditory neurons for both spectral and temporal parameters. Extracellular electrophysiology constituted an essential component, allowing for long-lasting, stable recordings of single- and multi-unit activity (cf. sections 2.3 and 2.5), while avoiding the penetration artifacts that have been reported for intracellular recordings (Ostrowski and Stumpner, 2014). Given this foundation, the response characteristics and temporal selectivity of prothoracic and

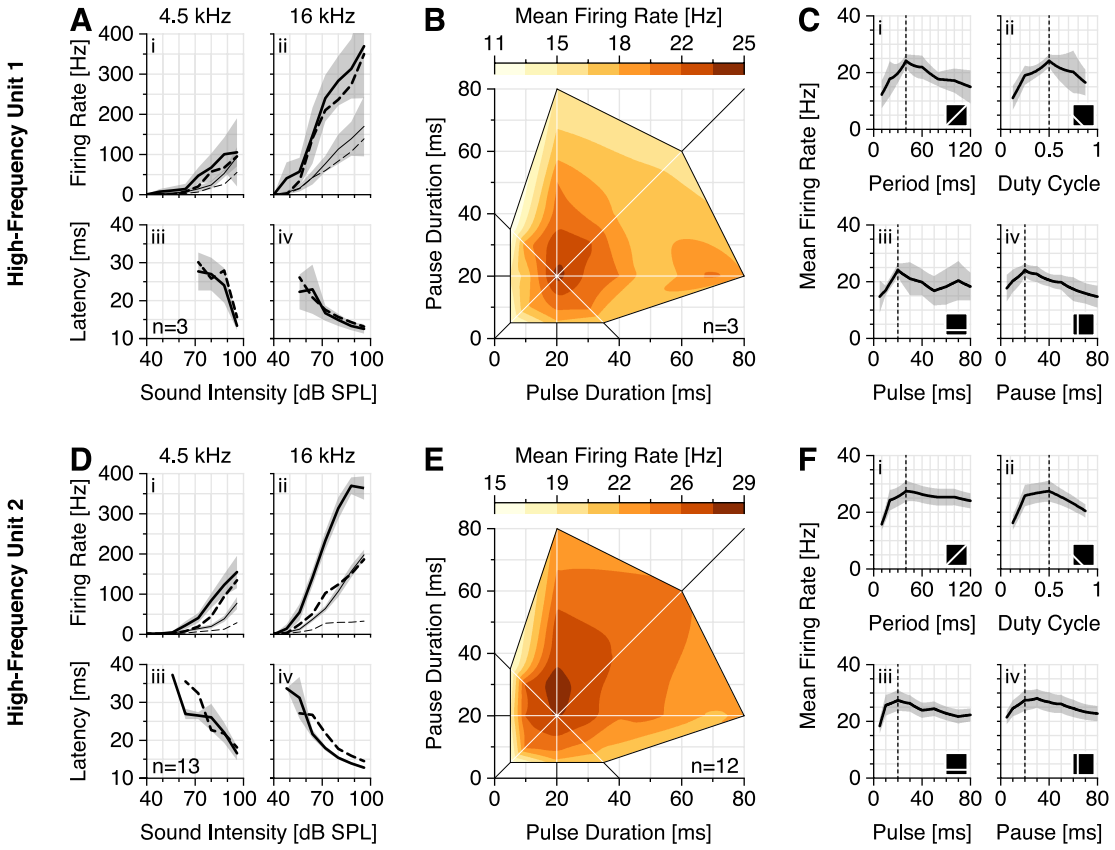

Figure 3.5 Pulse response properties of the high-frequency units HFU1 and HFU2. **A, D:** Average rate-intensity and latency-intensity functions at 4.5 kHz and 16 kHz CF. Responses to ipsilateral stimulation are indicated by solid lines; responses to contralateral stimulation by dashed lines. Thick lines represent the cells' onset response, whereas thin lines indicate their fully adapted steady-state response. The SEM is indicated in gray (only shown for ipsilateral responses). **B, E:** Average pulse response arrays at 4.5 kHz CF. **C, F:** Cross sections of the average pulse response arrays (black) and SEM (gray). Pictograms indicate the orientation of the respective cross section; dashed lines mark the parameters preferred by female crickets.

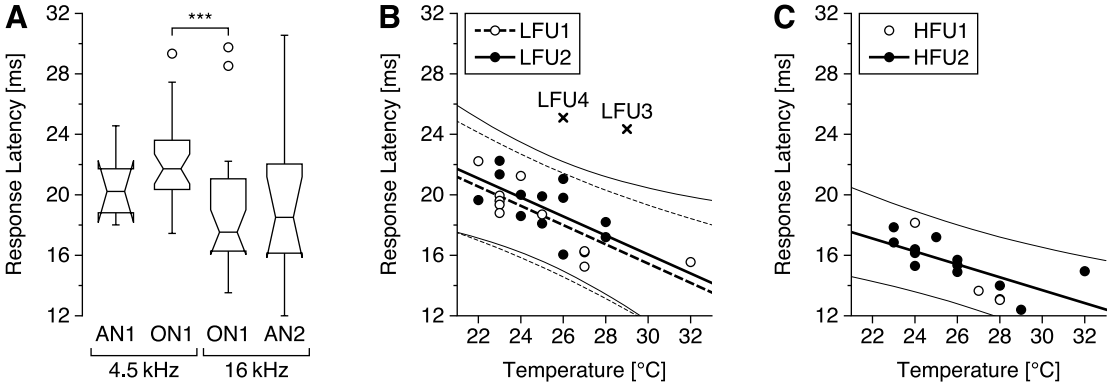

Figure 3.6 Dependence of response latencies on carrier frequency and temperature. **A:** First-spike latencies (FSLs) of prothoracic auditory neurons. Stimuli consisted of pure tone pulses with a square wave envelope, presented at 80 dB SPL. Circles indicate outliers; notches represent the 95 % confidence interval of the median. **B, C:** For units recorded within the cricket's brain, FSLs are shown as a function of the ambient temperature. Thick lines indicate linear regressions; thin lines represent the corresponding point-wise 95 % prediction bands. Data for LFU3, LFU4 and HFU1 could not be fitted due to the small sample-size. **B:** Low-frequency units, 4.5 kHz CF **C:** High-frequency units, 16 kHz CF.

suboesophageal auditory units could be characterized by means of exhaustive stimulation paradigms. The emerging "physiological fingerprints" were successfully used to distinguish between cell-types and partly compensated for the lack of morphological characterizations. As reported in previous studies, some neurons in the cricket's brain showed a sharp selectivity for the temporal characteristics of the conspecific calling song. Surprisingly, similarly matching, albeit weaker tuning could be shown for the prothoracic neuron AN2.

3.4.1 The Experimental Protocol

The study was based on two sets of acoustic stimuli. In the first set, simple tone pulses of increasing sound pressure level were used to assess the cells' rate-intensity and latency-intensity functions, yielding information about spectral and directional sensitivity, spike-frequency adaptation as well as response latency. A second set of stimuli was used to investigate the cells' processing of information in the temporal domain. It consisted of square-wave modulated pure tones with systematically varying pulse and pause durations. While most electrophysiological studies on this subject have only used periodical stimuli with a constant duty cycle of 0.5, the present study also included stimuli with other duty cycles. The resulting pulse response arrays allow for a more accu-

rate assessment of preferred song parameters and a better interpretability as to possible filter mechanisms (cf. Hennig et al., 2004).

Using the aforementioned measures, recorded units could be distinguished and pooled by their physiology alone. The response latency proved to be a particularly useful indicator for a sensory neuron's stage of processing, as it correlates with the "neuronal distance" between the upstream receptor and the neuron in question. Two principle factors determining a neuron's response latency are the conduction velocity along neurites (Hodgkin, 1954) as well as delays in the transduction processes of chemical synapses (Katz and Miledi, 1965b). While conduction delays increase in a continuous manner as a function of conduction distance, synaptic processes yield characteristic, stepwise increments in delay as the signal crosses cell boundaries. Thus, discrepancies in first-spike latencies in the order of several milliseconds are a strong indication for differences in cellular identity (cf. Schildberger, 1984).

3.4.2 Prothoracic Interneurons

Rate-intensity functions of the prothoracic interneurons (fig. 3.2) corroborate results of previous studies. The ascending neurons AN1 and AN2—widely regarded as providing the main auditory input to the cricket's brain (see Hennig, 1988 for review)—show complementary tuning for carrier frequencies (Boyan and Williams, 1982; Schildberger, 1984): AN1 is sharply tuned to low frequencies of about 4.5 kHz, with little to no activity during stimulation at 16 kHz. AN2, on the other hand, is primarily tuned to high carrier frequencies. This dichotomy reflects a processing in two separate frequency channels with opposing behavioral contexts: while AN1 modulates the positive phonotaxis towards calling songs of conspecific males (Schildberger and Hörner, 1988), AN2 processes aversive signals—the ultrasound calls of predatory bats (Nolen and Hoy, 1984). A third prothoracic unit, local interneuron ON1, had a wider carrier tuning and was sensitive to stimulation at both 4.5 kHz and 16 kHz; it was more sensitive to low-frequency stimuli by only about 10 dB (cf. Wohlers and Huber, 1978). It is associated with binaural contrast enhancement through lateral inhibition of both AN1 and AN2 (Selverston et al., 1985; Horseman and Huber, 1994a).

The three prothoracic neurons showed phasic-tonic responses at all stimulus intensities and carrier frequencies. The spike-frequency adaptation underlying this response type has been shown to introduce intensity invariance by means of high-pass filter properties (Benda and Hennig, 2008). In most situations, the unit was most sensitive to stimulations from the ipsilateral side. When stimulated at 16 kHz CF, however, AN2 responded more readily to stimulation from the contralateral side (fig. 3.2D_{ii}). This could be explained by the effects of sensory

adaptation: ipsilateral receptors are exposed to a higher stimulus amplitude than contralateral receptors and should therefor adapt more strongly. In extreme cases, this could yield an inversion of the interaural difference in response strength (Pollack, 2003). This explanation, however, is weakened by the fact that the contralateral lead appears to be most prominent in the onset response, that is, in the *unadapted* response. Furthermore, the effect was not observed for other units active in the high frequency regime. A more conservative explanation would be given by a miscalibration of the speakers' high-frequency output. This, however, can be ruled out, as the effect appeared irrespective of the recording's laterality (left or right connective) and using two separate experimental rigs.

Latency-intensity functions generally reflected the spectral tuning of the three cell-types. A closer look at a subset of response latencies revealed an interesting detail, as responses in the high-frequency channel had a lower latency than those in the low-frequency channel (fig. 3.6*A*). For ON1, the difference in response latency was significant, corroborating findings for *Teleogryllus oceanicus* (Pollack, 1994). This effect cannot be explained by physiological properties of the receptor neurons, as response latencies of high-frequency receptor populations are equal to (Pollack and Faulkes, 1998) or even higher than those of low-frequency receptor populations (Imaizumi and Pollack, 2001). Instead, Faulkes and Pollack (2001) suggested that the low-frequency response of ON1 might be delayed by a polysynaptic input through an unidentified non-spiking interneuron. This explanation, however, does not hold for the ascending neurons, as their afferents have been shown to be monosynaptic (Hennig, 1988). Here, differences in cellular anatomy could yield different conduction velocities, as AN2 has a particularly large axon diameter (Wohlers and Huber, 1985; Atkins and Pollack, 1986). This would also explain why latency differences between AN1 and AN2 are more pronounced when recorded in the cricket's brain, that is, after their respective APs have travelled a larger axonal distance (fig. 3.6 and section 3.4.3).

Pulse response arrays suggest remarkable differences in the temporal tuning of prothoracic auditory cells: While the firing rates of AN1 and ON1 mostly reflected the stimulus' duty cycle (fig. 3.2*B, H*), responses of AN2 indicated a moderate preference towards specific, behaviorally relevant stimulus parameters (fig. 3.2*E*). The present study thus questions the prevalent idea that ascending neurons merely relay auditory information to higher level processing and do not act as temporal filters themselves (Wohlers and Huber, 1982; Schildberger, 1984, 1988). While AN2 is usually linked to modulating evasive behavior in response to bat calls (Nolen and Hoy, 1984), several studies also support an involvement in mediating positive phonotaxis to songs of conspecifics (*G. bimaculatus*: Schildberger and Hörner, 1988; *A. domesticus*: Atkins et al., 1984, 1992). The results of the present study support and extend these findings, as they indicate that AN2

may not only act as a transmitter of phonotactically relevant information, but even exhibit behaviorally relevant filtering properties on its own.

3.4.3 Units Recorded in the Cricket's Brain

Physiological data suggest that the bulk of the units recorded in the cricket's brain were in fact ascending neurons. The most convincing evidence for this assumption is given by the units' consistently low response latencies (fig. 3.6). The apparent selection bias can be explained by several factors: While the temporal tuning of auditory neurons in the cricket's brain seems to increase with each processing stage, firing rates generally decrease (cf. Schildberger, 1984). Due to their lower firing rates, higher level units are less likely to be detected in extracellular multi-unit recordings than the more conspicuously active ascending neurons. Furthermore, the probing for units was performed during stimulation with constant tone pulses of 500 ms duration. This could further complicate the detection of higher order brain neurons, as these have a preference for temporally patterned sounds. Finally, cellular anatomy could also contribute to a selection bias: if higher level units had particular low diameter axons, they would produce weaker extracellular potentials—which, consequently, would make them harder to record from extracellularly.

LFU1 and LFU2 most likely are physiological variations of AN1: both units featured a clear preference for low carrier frequencies, responded with short latencies and exhibited a strong dependence on the stimulus' duty cycle (figs. 3.3 and 3.6). The only notable physiological difference between the two units was observed at high carrier frequencies: here, LFU2 exhibited a considerable response towards ipsilateral stimulation (fig. 3.3D_{ii}). At intermediate stimulus intensities, this response lacked a defined onset component, suggesting that it was partially masked by an adapting inhibitory input—most likely through ON1 (Horseman and Huber, 1994a). Altogether, the characteristics of LFU1 and LFU2 corroborate the findings of Schildberger (1984), who described two individual physiological variants of AN1 with differentially expressed inhibitory sidebands. In a similar vein, HFU1 and HFU2 seem to be physiological variations of AN2—again, with the only difference being the directional sensitivity towards high CF stimuli (fig. 3.5). The occurrence of comparable response variations in both AN1 and AN2 suggests that these variations may originate from a common afferent—that is, either ON1 or a high-frequency receptor type.

LFU3 and LFU4 appear to be "true" brain neurons, as both exhibited considerably higher response latencies than the ascending neurons AN1 and AN2 (fig. 3.6*B*). The two units' latencies were similar to those of the previously described, early brain neurons BNC1 (Schildberger, 1984, fig. 6; 22 ms to 25 ms

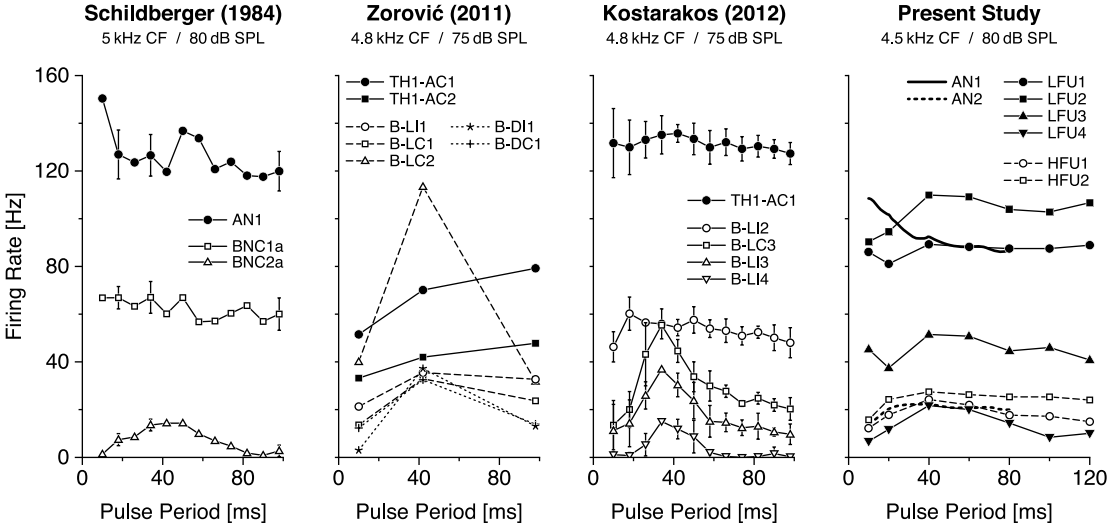

Figure 3.7 Preferences for patterns with varying pulse periods compared to data from previous studies. In all cases, stimuli had a duty cycle of 0.5. Data in the first three panels originate from studies by Schildberger (1984); Zorović and Hedwig (2011) as well as Kostarakos and Hedwig (2012). Note, how an increase in selectivity coincides with a decrease in firing rate. TH1-AC1 corresponds to AN1; TH1-AC2 to AN2. Error bars: SD.

latency) and B-LI2 (Kostarakos and Hedwig, 2012; 24.6 ms latency). Unlike AN1, the two units' responses did not strictly correlate with the stimulus duty cycle. Instead, they featured a clear selectivity for the calling song parameters of *G. bimaculatus* (fig. 3.4*B*, *E*). The responses of LFU3 indicated overall similar firing rates as BNC1 and B-LI2, but exhibited a slightly stronger tuning for behaviorally relevant pulse periods (fig. 3.7). LFU4 exhibited lower firing-rates and stronger temporal tuning than LFU3, and—except for its much lower latency—was similar to BNC2a, described by Schildberger (1984).

Altogether, the stimulus selectivity of auditory neurons increased in sequence of processing, while firing rates decreased, corroborating evidence from previous studies (fig. 3.7; Schildberger, 1984; Zorović and Hedwig, 2011; Kostarakos and Hedwig, 2012). This trend towards a sparse representation of information is reminiscent of the labeled line code proposed for the auditory system of grasshoppers (Clemens et al., 2011).

3.4.4 Conclusion

I employed a comprehensive stimulus set of square-wave modulated tones to differentiate extracellularly recorded units throughout the cricket's auditory system and to characterize their processing of temporally structured sound. The stimu-

lation paradigm allowed for a detailed analysis of the units' filtering properties regarding pulse patterns with different periods and duty cycles. Results from previous studies on the cricket's auditory system suggested a gradual increase in stimulus selectivity, accompanied by a drecrease in firing rate as the sound information moves towards higher-order neurons (fig. 3.7; Schildberger, 1984; Zorović and Hedwig, 2011; Kostarakos and Hedwig, 2012). My findings confirm these trends. By covering a more extensive parameter space, however, I was able to disclose further details: Already on the level of the auditory periphery, two fundamentally different response classes emerged, reflecting either the stimuli's duty cycle (AN1, ON1) or a preference for the species' calling song parameters (AN2, LFU3, LFU4). The most notable result of the present study is the surprisingly articulate tuning of the peripheral neuron AN2, which is comparable to that of previously described brain neurons (B-LI1 and B-LC1 of Zorović and Hedwig, 2011; cf. fig. 3.7). The findings suggest that the prothoracic auditory neurons do not merely act as transmitters of phonotactically relevant information, but rather exhibit behaviorally relevant filtering properties on their own.

4 Modulation Transfer Functions of Prothoracic Auditory Neurons

4.1 Introduction

In the previous chapter, I described an explorative approach of surveying the cricket's auditory system. It aimed at obtaining "physiological fingerprints" of extracellularly recorded auditory neurons by covering a wide array of temporally patterned sound stimuli. Unexpectedly, the results suggested the presence of firing-rate resonances at an early level of processing and thus prompted a closer look at the modulation transfer characteristics of prothoracic auditory neurons.

The combination of acoustic stimulation and extracellular recordings from auditory cells corresponds to a "black box" approach: A neuronal system is analyzed irrespective of its actual implementation by merely relating its input to its output. Given a linear system, this transformation is fully described by the system's transfer function. Correspondingly, a neuronal system's processing of amplitude modulated (AM) sound is described by its modulation transfer function (MTF): It is obtained by systematically varying the envelope function of a sound stimulus and relating it to the neuronal response (cf. fig. 1.2*A*).

In the previous chapter, the pattern selectivity of auditory cells was probed with square wave modulated pure tones—a stimulus paradigm that was established as a simplifying but adequate analogy to the cricket song during behavioral experiments (Popov and Shuvalov, 1977). While square wave stimuli are readily defined in terms of pulse and pause durations, they have a decisive drawback for systems analysis: in the frequency domain, square waves have a wide range of harmonics. To analyze the neuronal processing of time-varying sounds, stimuli with a sinusoidal amplitude modulation (SAM) have become widely adopted instead. SAM stimuli consist of only two frequencies: the sine carrier and the lower frequency sine modulator (Malone and Schreiner, 2010).

The output of a neuronal system is usually characterized by the occurrence of a discrete physiological signal, the action potential (AP). There are two basic

coding schemes by which a sequence of APs could represent information: first, by the number of APs that occur within a particular time period, or second, by the precise timing of individual APs (Gerstner et al., 1997). In auditory science, these fundamental aspects of neuronal communication are addressed by two common measures: the *rate* modulation transfer functions (rMTF) and the *temporal* modulation transfer functions (tMTF) (Malone and Schreiner, 2010).

In this chapter, I combine extracellular electrophysiology with a novel stimulation paradigm: the swept-frequency amplitude modulated (SFAM) stimulus. It builds on the concept of the SAM stimulus but allows for a more efficient collection of data by sweeping through a defined range of AM frequencies in a short time period. Various measures used in the context of SAM stimuli were revised with respect to this new paradigm. I utilized this tool set to obtain detailed modulation transfer functions of the cricket's prothoracic auditory neurons. The results confirmed the presence of behaviorally relevant, tuned firing-rate resonances in the cricket's peripheral auditory network.

4.2 Methods

This section only details methods specific to the present study. For a description of the more general methods involved, refer to chapter 2, sections 2.1 to 2.6.

4.2.1 Stimulus Design

To efficiently sample both spike rate and spike timing responses across a range of frequencies, I employed acoustic stimuli with a swept-frequency amplitude modulation (SFAM). The envelope function of SFAM stimuli resembled a sinusoidal wave whose instantaneous frequency $f_{\mathrm{AM}}(t)$ changed linearly with time:

$$\begin{aligned} f_{\mathrm{AM}}(t) &= f_0 + \beta t, \\ \beta &= \frac{f_1 - f_0}{t_1}, \end{aligned} \tag{4.1}$$

where f_0 was the initial frequency at time $t = 0\,\mathrm{s}$, f_1 was the target frequency at stimulus duration t_1 and β was the sweep rate; that is, the slope of $f(t)$. The amplitude of the envelope function followed:

$$y(t) = \frac{1}{2}\cos\left[2\pi\left(f_0 t + \frac{\beta}{2}t^2\right) + \pi\right] + \frac{1}{2}.$$

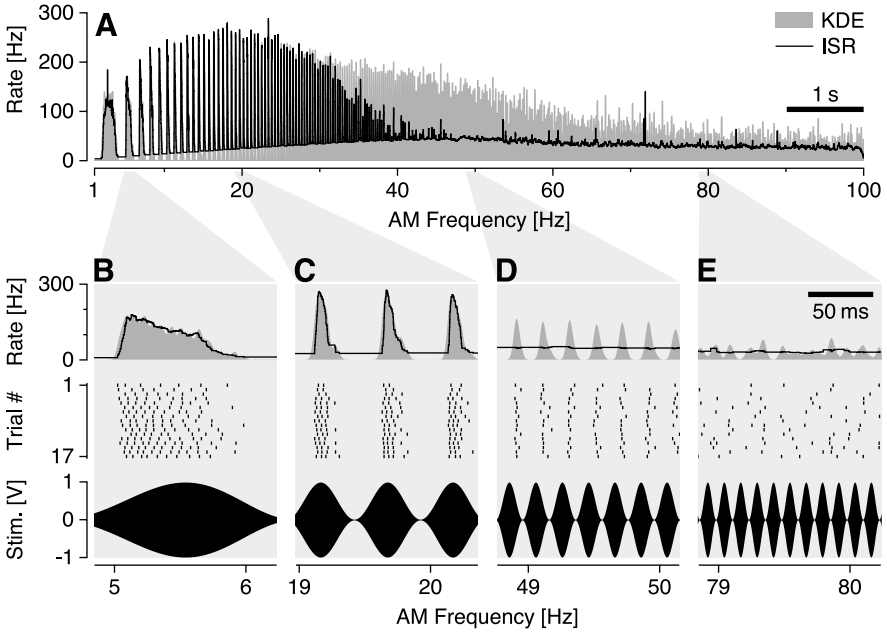

Figure 4.1 Exemplary response of ON1 to a 10 s SFAM stimulus rising in AM frequency from 1 Hz to 100 Hz (80 dB SPL, 4.5 kHz CF). **A:** kernel density estimation (KDE, gray) overlaid with average instantaneous spike rate (ISR; black) across 17 trials. Selected periods are expanded in panels **B–E**. Each of them shows (from top to bottom): KDE (gray) overlaid with average ISR (black), a spike raster plot and the respective section of the stimulus. **B:** Spike-frequency adaptation erodes the response. **C:** High firing rates, several spikes per stimulus period. **D:** Stimulus-locked firing at low overall spike rates. **E:** Desynchronized firing at low spike rates.

Stimuli with the parameters $t_1 = 10\,\mathrm{s}$, $f_0 = 1\,\mathrm{Hz}$ and $f_1 = 100\,\mathrm{Hz}$ were used, which resulted in a sweep rate of $\beta = 9.9\,\mathrm{Hz\,s^{-1}}$. For AN1 and AN2, additional stimuli were used, having a shorter duration ($t_1 = 5\,\mathrm{s}$) and frequencies ranging from $f_0 = 0\,\mathrm{Hz}$ to either $f_1 = 50\,\mathrm{Hz}$ or $f_1 = 500\,\mathrm{Hz}$ (yielding sweep rates of $\beta = 10\,\mathrm{Hz\,s^{-1}}$ and $\beta = 100\,\mathrm{Hz\,s^{-1}}$, respectively). To account for effects of adaptation, stimuli were also presented in reverse, that is, with falling instantaneous frequencies. Envelope functions were multiplied with sine carriers of either 4.5 kHz or 16 kHz, accounting for the different spectral sensitivities of AN1, AN2 and ON1 (Popov et al., 1976; Boyan and Williams, 1982). Stimuli were presented in randomized order with each stimulus being presented up to 25 times, depending on the state of the recording.

4.2.2 Modulation Transfer Functions

The SFAM stimulation protocol delivered a linear sweep of modulation frequencies, with each stimulus segment representing a defined frequency band. This

property was exploited by analyzing the experimentally obtained data with a sliding window approach. The procedure yielded two measures, the *rate* modulation transfer function (rMTF) and the *temporal* modulation transfer function (tMTF), characterizing AM frequency transfer on the levels of both firing rate and stimulus locking (Eggermont and Wang, 2011).

In order to obtain these two kinds of MTFs, I first converted the recorded spike times into binary spike trains (waveforms at the 20 kHz sampling rate of the original recordings with *zero* representing *"no spike"* and *one* representing *"spike"*). These row vectors were averaged across trials and multiplied by their sampling rate, essentially yielding the numerical representation of a highly resolved peristimulus time histogram (PSTH; Gerstein and Kiang, 1960) with a bin size equal to the reciprocal of the recording's sampling rate.

From this data, both the rMTF and the tMTF could be determined as spectrotemporal measures by means of the short-time Fourier transform (STFT)—a Fourier-related transform that captures the spectral properties of a local section of a signal. The discrete STFT corresponds to a regular discrete Fourier transform (DFT) but combines the sampled signal $x(m)$ with a window function $w(m)$:

$$X(n,k) = \sum_{m=0}^{N-1} x(m)w(n-m) \cdot e^{-i\frac{2\pi}{N}km}, \qquad k \in \mathbb{Z},$$

where $f(m) = x(m)w(n-m)$ is a short-time section of signal $x(m)$ at time n, N is the length of $x(m)$ and k is the index of the DFT coefficient to be calculated.

The *rate* modulation transfer function (rMTF) describes a cell's mean firing rate as a function of AM frequency (Schreiner and Langner, 1988). In the frequency domain, the mean value of a signal is given by the spectral magnitude at 0 Hz—the so-called DC bias. The corresponding STFT at $k = 0$ reduces to a convolution of signal x and window w:

$$\begin{aligned} \mathrm{rMTF}(t) &= |X(t f_s, 0)|, \\ &= \sum_{m=0}^{N-1} x(m)w(t f_s - m), \end{aligned}$$

where f_s is the sampling rate of the recording. Thus, in this case the STFT was merely used for smoothing the highly resolved PSTH from the previous step.

The *temporal* modulation transfer function (tMTF) characterizes a cell's ability to synchronize its firing to the amplitude modulations of a stimulus (Schreiner and Langner, 1988). It can be expressed both in absolute or relative terms (Eggermont and Wang, 2011). The relative measure is commonly known as the

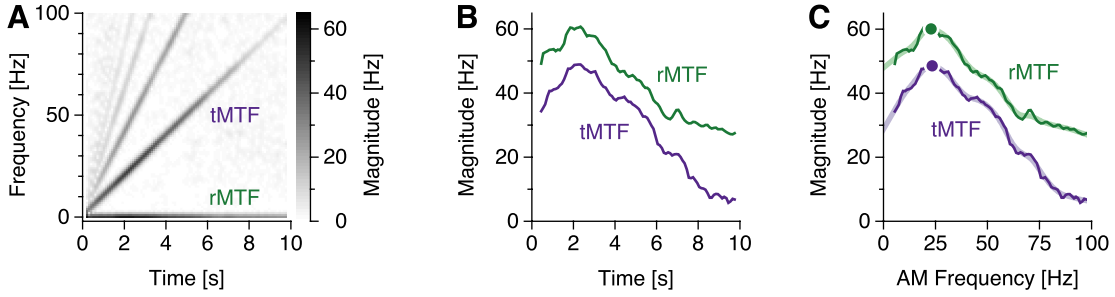

Figure 4.2 Modulation transfer functions. **A:** Spectrogram of the spiking response to an SFAM stimulus (average of 17 repetitions, same data as in fig. 4.1). The cell's rate modulation transfer function (rMTF) corresponds to the spectrogram's DC component. The temporal modulation transfer function (tMTF) is given by the cross-section of the spectrogram along the stimulus' rising fundamental frequency. It represents the absolute rate contribution of stimulus locked spikes. **B:** rMTF and tMTF from the spectrogram. **C:** The time axis was replaced by its corresponding axis of modulation frequency. Data was smoothed by means of cubic smoothing splines (broad lines) to ease the automated detection of transfer peaks in individual recordings. Detected peaks: 23.0 Hz (rMTF) and 23.5 Hz (tMTF); Q values: 1.25 and 1.69, respectively (filled circles).

vector strength (VS; see section 4.2.3). Here, however, the tMTF is defined as an absolute measure of phase-locked firing rate; that is, the magnitude of the response's Fourier component at the stimulus' instantaneous AM frequency:

$$\mathrm{tMTF}(t) = \left|X[t\, f_s, k_{\mathrm{AM}}(t)]\right|,$$

where $k_{\mathrm{AM}}(t)$ is the DFT index that corresponds to the stimulus envelope's instantaneous frequency $f_{\mathrm{AM}}(t)$ (see eq. 4.1):

$$k_{\mathrm{AM}}(t) = \left\lfloor N \cdot \frac{f_{\mathrm{AM}}(t)}{f_s} \right\rfloor.$$

For both MTFs, I used a flat top window (Gade and Herlufsen, 1987) of width $\sigma = 1\,\mathrm{s}$ (for $\beta \leq 10\,\mathrm{Hz\,s^{-1}}$) or $\sigma = 300\,\mathrm{ms}$ (for $\beta = 100\,\mathrm{Hz\,s^{-1}}$) and 90 % overlap. The Goertzel algorithm was employed for an efficient and accurate evaluation of the individual DFT terms (Goertzel, 1958; Sysel and Rajmic, 2012, section 3.4). The two measures correspond to cross-sections of the spike train's magnitude spectrogram along the DC component and along the stimulus envelope's fundamental frequency (cf. fig. 4.2). While the rMTF quantifies mean spike rates much like a regular PSTH, the tMTF represents the absolute rate contribution of spikes that are phase-locked to the stimulus' instantaneous frequency.

4.2.3 Vector Strength

The vector strength (VS) was used as a relative measure of a cell's capability to phase-lock to the amplitude modulations of a stimulus. It was calculated by normalizing the tMTF by the rMTF (Eggermont and Wang, 2011):

$$\mathrm{VS}(t) = \frac{\mathrm{tMTF}(t)}{\mathrm{rMTF}(t)}.$$

If all APs occur at the same phase within the AM period, the VS will equal 1; if they are uniformly distributed across the AM period, the VS will equal 0. The significance of phase locking was assessed by means of the Rayleigh test for circular distributions (Zar, 1999):

$$z(t) = n_{\mathrm{spikes}}(t) \cdot \mathrm{VS}(t)^2,$$

where n_{spikes} is the number of spikes per modulation period across all trials, obtained by multiplying the rMTF with the number of trials and dividing by the instantaneous frequency $f(t)$:

$$n_{\mathrm{spikes}}(t) = \frac{\mathrm{rMTF}(t) \cdot n_{\mathrm{trials}}}{f_{\mathrm{AM}}(t)}.$$

The significance threshold was set to $z = 3$, corresponding to $p = 0.05$ (Zar, 1999).

4.2.4 Detection and Characterization of Transfer Peaks

The position and shape of transfer peaks were characterized on a per-experiment basis. To this end, rMTFs and tMTFs were fitted with cubic smoothing splines (smoothing parameter $p = 0.02$, average $R^2 = 0.99$), extrapolated to 0 Hz and processed with a peak detection algorithm (Todd and Andrews, 1999). Peaks in the smoothed MTFs were included in further analyses, if they rose above adjacent troughs by an amplitude factor of 1.1 or higher. They were characterized by the peak frequency f_{p} and the quality factor Q, the latter defined as the ratio of the magnitude at f_{p} to the extrapolated magnitude at 0 Hz (Koch, 1984).

4.2.5 Simulation of Suboptimal Spike Sorting

In amplitude-based spike sorting one tries to separate units by their distributions of spike amplitudes (cf. section 2.5.1). If amplitude distributions overlap, one faces a trade-off between accepting false positive spikes (type I error; fig. 4.3*A*) and rejecting "true" spikes (type II error; fig. 4.3*B*). This situation is a common

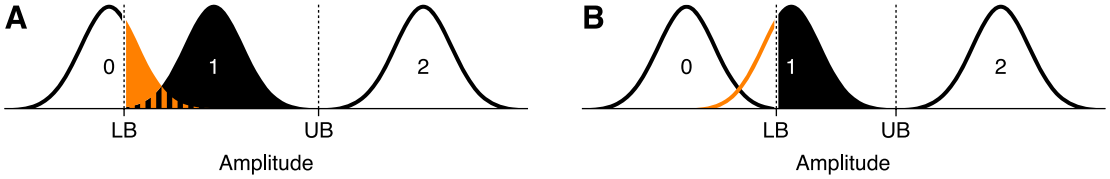

Figure 4.3 Overlapping feature distributions lead to classification ambiguity. The problem is illustrated by a hypothetical amplitude distribution 1, which is to be separated from two adjacent distributions 0 and 2 by lower and upper amplitude bounds (LB and UB). A trade-off between two types of classification errors arises: **A:** All elements from distribution 1 can be registered, if the lower bound is set accordingly. This, however, comes at the cost of accepting false-positive elements from the overlapping distribution 0 (type I error). **B:** False-positives can only be avoided by raising the lower bound—leading to the incorrect rejection of low amplitude elements from distribution 1 (type II error).

problem for extracellular recordings of AN1 (Faulkes and Pollack, 2000). To illustrate the impact of the aforementioned spike sorting errors on the performance of MTFs and VS, I conducted a simulation: A clean recording of ON1 (SFAM stimulation between 1 Hz and 100 Hz, 4.5 kHz CF, 20 repetitions) was subjected to controlled degradation by either adding or removing spikes.

Type I errors were simulated by adding non-stimulus related spike events to the original dataset. This was achieved by means of a gamma process (Nawrot et al., 2008); that is, random ISIs were drawn from a gamma distribution whose probability density function (PDF) is defined as

$$f_{\alpha,\rho}(x) = \begin{cases} \frac{1}{\Gamma(\alpha)} \rho (\rho x)^{\alpha-1} e^{-\rho x}, & x \geq 0, \\ 0, & x < 0, \end{cases}$$

where Γ denotes the gamma function. The process is determined by gamma order $\alpha > 0$ and rate parameter $\rho > 0$, with the mean rate λ given by

$$\lambda = \frac{\rho}{\alpha}.$$

The gamma order was set to $\alpha = 5$ and the rate parameter to $\rho = 75$, 150 or 225, resulting in mean rates of 15 Hz, 30 Hz or 45 Hz respectively. The renewal process was given a 40 s "warm-up" period to avoid the high inter-trial correlations at simulation onset (equilibrium conditions; Tuckwell, 2005; Nawrot et al., 2008).

Type II errors were simulated in a separate approach by omitting a random subset of the "true" spike events. In this manner, the exemplar dataset of ON1 was thinned out by either 20 %, 40 % or 60 %.

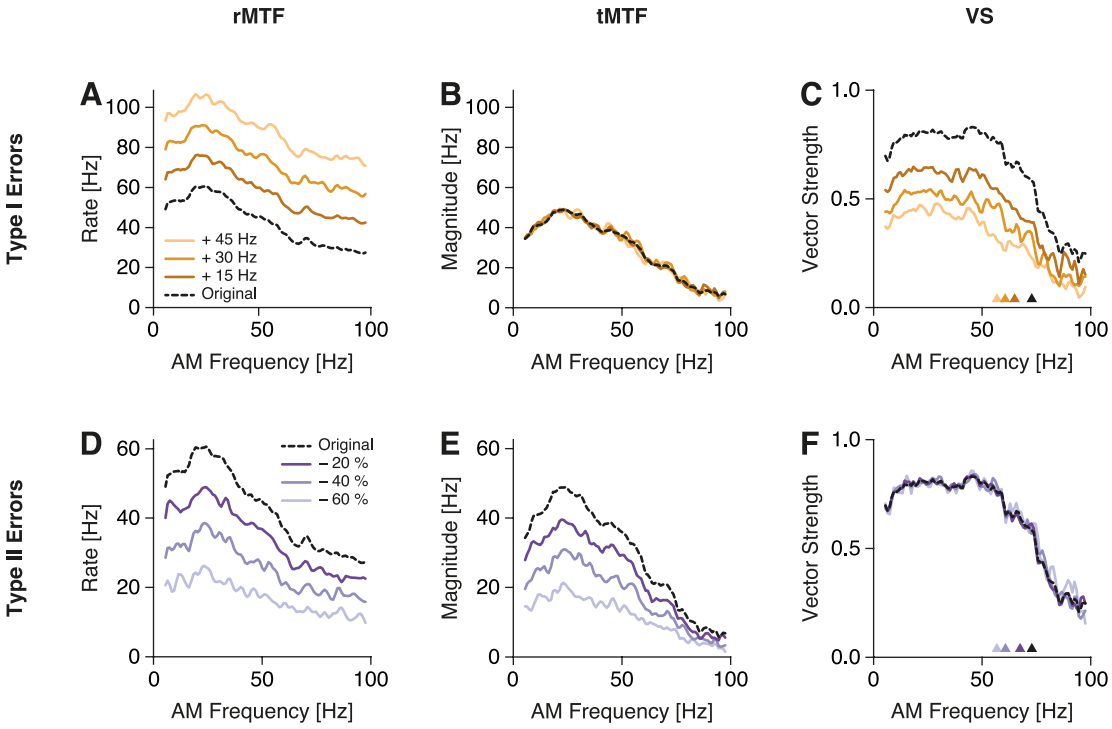

Figure 4.4 The impact of suboptimal spike sorting on the performance of modulation transfer functions and vector strength. Triangles mark the AM frequencies at which phase locking fell below the 5 % significance level. **A–C:** Effect of false positive spike classifications (type I errors). **D–F:** Effect of missed spikes (type II errors).

On the basis of the degraded spiketrains, MTFs and VS were calculated using the routines described in sections 4.2.2 and 4.2.3. The manipulations' impact on the three measures was evaluated in a qualitative manner through comparison with the unaltered data.

4.3 Results

In order to investigate the occurrence of firing-rate resonances in the auditory periphery of crickets, I obtained modulation transfer functions (MTFs) for three auditory cell types in the prothoracic ganglion of *G. bimaculatus*: The ascending neurons AN1 and AN2 that form the main input for auditory processes in the cricket brain (Boyan and Williams, 1982; Schildberger, 1984; Hennig, 1988) as well as the local interneuron ON1 that laterally inhibits AN1 and AN2 (Selverston et al., 1985; Horseman and Huber, 1994a). The frequency tuning of these cell types was characterized by means of extracellular recordings combined with acoustic stimulation by swept-frequency amplitude modulated (SFAM) tones.

The SFAM stimulation protocol is exemplified in fig. 4.1*A* with an illustrative recording of ON1. Here, the stimulus consisted of a tone of 4.5 kHz carrier frequency with a sinusoidal amplitude modulation sweeping through frequencies of 1–100 Hz within 10 s. It covered a frequency range of particular relevance to the cricket: The ~25 Hz characteristic of the pulsed mating song of male conspecifics. ON1's responses to lower frequency stimulus components (fig. 4.1*B*) were attenuated by spike frequency adaptation. Firing rates increased with modulation frequencies up to around 20 Hz (fig. 4.1*C*), after which they started to decline again, with fewer spikes fitting the gradually contracting modulation periods of the stimulus (fig. 4.1*D*). Eventually, at very high modulation frequencies, the cell decoupled from the stimulus and fired erratically at low overall rates (fig. 4.1*E*). Altogether, the cell's response exhibited band-pass tuning in the range of the behaviorally relevant frequencies.

Two measures were extracted from the magnitude spectrogram of the response spike trains: the rate modulation transfer function (rMTF) and the temporal modulation transfer function (tMTF) (fig. 4.2*A*). Given SFAM stimulation, the two measures corresponded to the magnitude spectrogram's DC bias (rMTF) and its magnitude at the instantaneous stimulus frequency (rMTF). While the rMTF indicates mean firing rates much like a PSTH (Gerstein and Kiang, 1960), the tMTF represents only the rate contribution of stimulus locked spikes. A cell's decoupling from a stimulus is therefore reflected in the divergence of the two measures—observed, for example, at high AM frequencies (fig. 4.2*B*). The divergence of rMTF and tMTF is captured by their quotient, the so called vector strength (acsvs; not shown). To facilitate the algorithmic detection and characterization of firing-rate resonances within individual MTFs, the latter were fitted with cubic smoothing splines (fig. 4.2*C*).

To test the impact of suboptimal spike sorting on the performance of MTFs and VS, an SFAM dataset was subjected to controlled degradation. The effect of false positive spike classifications (type I errors) was explored by adding random events to the original spike trains. The rMTF was uniformly raised by the mean rate of the inserted spikes (fig. 4.4*A*). Being uncorrelated with the AM of the stimulus, the inserted spikes had no influence on the tMTF (fig. 4.4*B*). Through the additive increase of the rMTF—the divisor in the definition of the VS—the latter was scaled unproportionally (fig. 4.4*C*). In a separate approach, the effect of missed spikes (type II errors) was investigated by omitting a random subset of "true" spikes from the original dataset. Both rMTF and tMTF were proportionally scaled by the fraction of spikes remaining (fig. 4.4*D*, *E*). The omission of spikes had no effect on the VS, because it affected rMTF and tMTF in equal parts and ultimately cancelled out (fig. 4.4*F*). The significance of phase locking, however, dropped.

Figure 4.5 shows the modulation transfer functions of AN1, AN2 and ON1, averaged across all recordings. Due to the high baseline activity often evident in hook electrode recordings of AN1 (Faulkes and Pollack, 2000), the cell's rMTF could not be derived reliably (fig. 4.5*A*). This is also reflected in an overall low vector strength, which did not exceed values of 0.6 (fig. 4.5*G*). AN1's tMTF was relatively flat with no indications for sharp band-pass tuning (fig. 4.5*D*). AN2 showed clear firing-rate resonances, peaking at modulation frequencies of around 30 Hz to 40 Hz (fig. 4.5*B, E*). Its rMTF had a slightly increased peak frequency with respect to its tMTF. AN2's vector strength had a sharp peak at approximately 30 Hz, reaching values of 0.8–0.9 (fig. 4.5*H*). The two MTFs of ON1 exhibited a more pronounced drop-off at higher modulation frequencies than AN2; for both measures, distinct band-pass tuning was observed, with peak frequencies at approximately 25 Hz (fig. 4.5*C, F*). Stimuli with a high carrier frequency resulted in a sharper tuning than those with a low carrier frequency. For both stimulus conditions, ON1's vector strength exceeded values of 0.9 (fig. 4.5*I*).

In addition to the MTFs averaged across individuals, firing-rate resonances were characterized on the basis of single recordings. Here, peaks in the MTFs were detected algorithmically and characterized by their respective frequency and Q value[1], as summarized in figure 4.6 and table 4.1.

4.4 Discussion

4.4.1 The Experimental Protocol

To assess an auditory neuron's frequency transfer at the level of firing rates, I conceived of a straightforward protocol that uses acoustic stimuli sweeping through a range of modulation frequencies (figs. 4.1 and 4.2). The approach draws inspiration from the ZAP protocol, which is used to assess the frequency dependence of subthreshold voltage responses in single cells (impedance amplitude profile; Gimbarzevsky et al., 1984; Hutcheon and Yarom, 2000; Schreiber et al., 2004). In contrast to the latter approach, however, I here characterize a neuron's *suprathreshold* firing rate responses to *cell-external* stimuli. Thus, the observed frequency characteristics are not shaped by the recorded cell's subthreshold properties alone, but also by properties of its spike generating mechanism and upstream network. The protocol has several general advantages with relevance to this study: First, SFAM stimuli can assess a broad range of modulation frequencies using relatively short stimuli. It thus provides a better consistency in

[1] Note: the Q value characterizes the low-frequency drop-off of a filter—it does not capture differences in the high-frequency drop-off (as observed for the average MTFs).

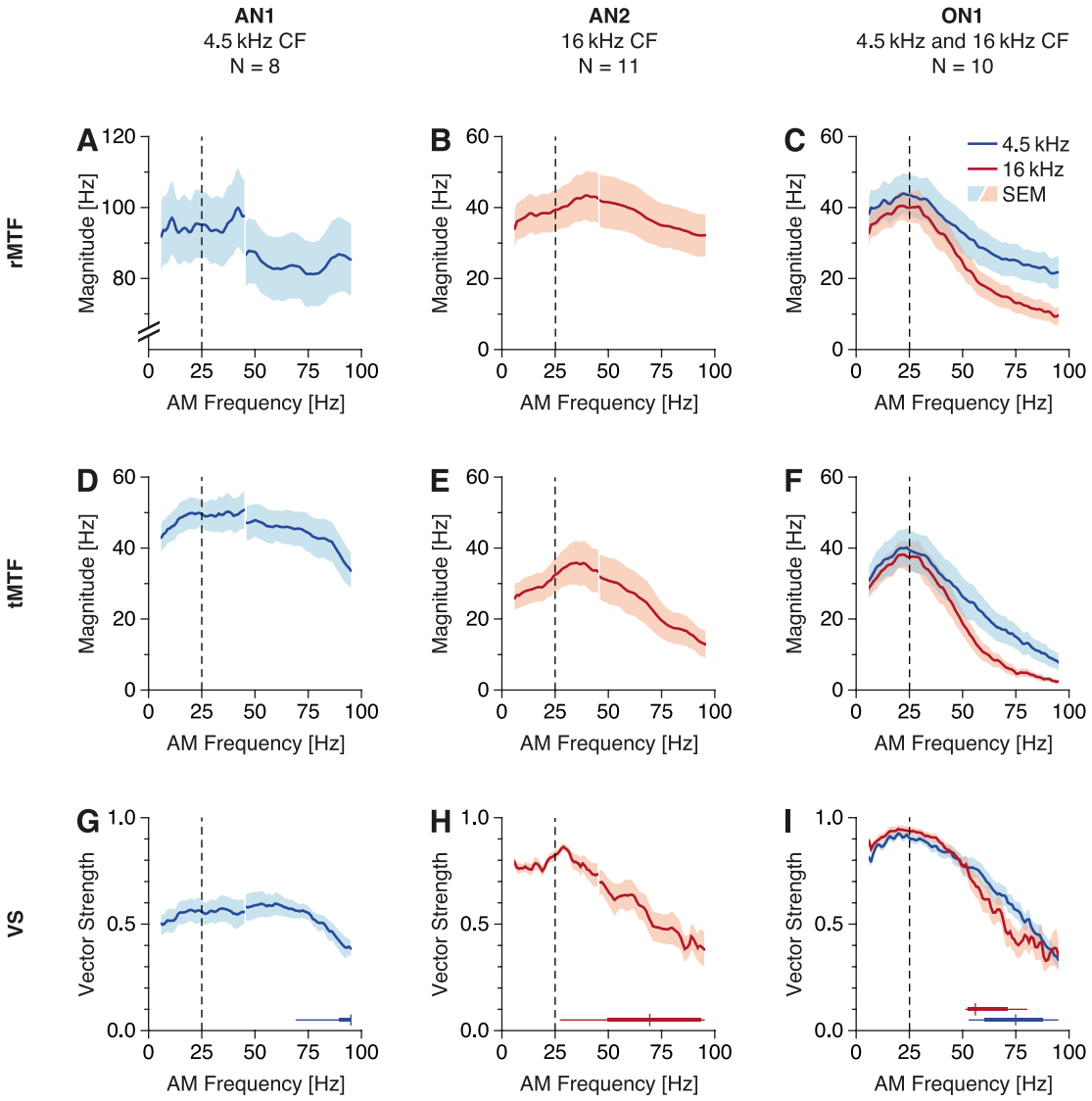

Figure 4.5 Average modulation transfer functions (MTFs) of the prothoracic interneurons AN1, AN2 and ON1. Dashed lines indicate the 25 Hz pulse frequency typical for songs of *G. bimaculatus*; N denotes the number of recordings for the respective cell type. Panels for AN1 and AN2 comprise two sets of stimuli with different frequency ranges, hence the apparent seam in the respective MTFs. **A–C:** Rate MTFs. Note the discontinuous y-axis for AN1. **D–F:** Temporal MTFs. **G–I:** Vector strength (VS). Horizontal box plots indicate the AM frequencies at which the VS of individual recordings fell below the 5 % level.

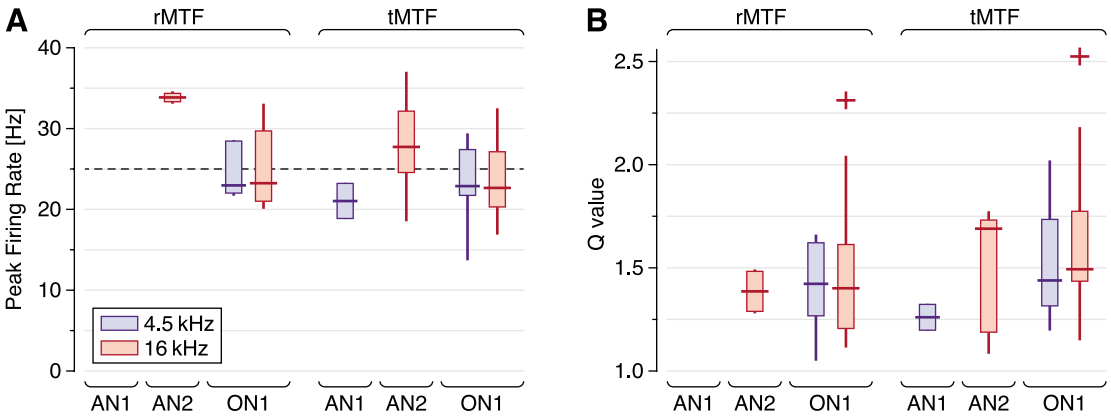

Figure 4.6 Characterization of modulation transfer functions based on individual recordings. **A:** Peak frequencies of detected transfer peaks. The dashed line indicates the 25 Hz pulse frequency typical for songs of *G. bimaculatus*. **B:** The corresponding Q values. Crosses indicate outliers.

Table 4.1 Modulation Transfer in Individual Recordings.

			rMTF			tMTF		
Type	f_c [kHz]	N	n_p	$\widetilde{f}_p$ [Hz]	$\widetilde{Q}$	n_p	$\widetilde{f}_p$ [Hz]	$\widetilde{Q}$
AN1	4.5	8	0	—	—	2	21.0	1.26
AN2	16.0	11	2	33.8	1.38	5	27.7	1.69
ON1	4.5	10	6	22.9	1.42	10	22.8	1.44
ON1	16.0	10	9	23.2	1.40	10	22.6	1.49

f_c denotes the carrier frequency, N the number of recordings, n_p the number of recordings with detected transfer peaks. $\widetilde{f}_c$ and $\widetilde{Q}$ denote the median peak frequency and median Q value of the respective peaks.

recording conditions and an overall reduced recording time, when compared to stimuli with a constant modulation frequency (Farris et al., 2004; Schildberger, 1984; Zorović and Hedwig, 2011). Second, the protocol implements commonly used measures for quantifying both mean and stimulus-locked firing rates; that is, both *rate* and *temporal* modulation transfer functions, vector strength and circular statistics. Third, since they involve a pulse-like amplitude modulation, SFAM stimuli are still fairly close to the cricket's natural song, while avoiding the harmonic distortions typical for square-wave modulated sounds. Fourth, the protocol is robust; it does not require averaging across individuals and yields valid modulation transfer functions, even for extracellular recordings with very low signal-to-noise ratios.

4.4.2 Firing-rate Resonances and Behavioral Relevance

The auditory pathway of the cricket is a dedicated system designed to detect and localize two classes of objects: mating partners and predators, most prominently bats. Peripheral frequency filtering and object categorization are well known mechanisms by which these tasks are accomplished (Wohlers and Huber, 1978; Wyttenbach et al., 1996; Hildebrandt, 2014). The ascending neurons AN1 and AN2 have differential tuning for low and high carrier frequencies, respectively (cf. chapter 3; Wohlers and Huber, 1978; Hennig, 1988), and are known to influence behavior (for AN1: Schildberger and Hörner, 1988; for AN2: Nolen and Hoy, 1984; Marsat and Pollack, 2006). Thus, these neurons likely represent the two channels of information transfer associated with categorical perception. In contrast, the function of ON1 is usually attributed to localization (Selverston et al., 1985). Because ON1 exhibits wide carrier tuning, it affects both transmission channels.

The modulation transfer functions of AN1 did not exhibit a clear tuning to the 25 Hz pulse rate of the calling song of *G. bimaculatus* (fig. 4.5*A, D*, table 4.1), which corresponds with results both from chapter 3 and from previous studies on crickets with lower or higher pulse rates (*T. oceanicus*: Benda and Hennig, 2008, *G. assimilis*: Pollack and Kim, 2013). Distinct temporal selectivity for the conspecific pulse rate apparently arises at higher stages; indeed, in brain neurons, hierarchical tuning has been reported (Schildberger, 1984; Kostarakos and Hedwig, 2012). Unlike the protocol used in chapter 3, the modulation transfer functions derived from SFAM stimuli revealed strong firing-rate resonances for ON1 that matched the temporal characteristics of the conspecific calling song. While ON1's primary role is generally considered to be contrast enhancement of binaural localization cues rather than pattern recognition, its temporal tuning at low carrier frequencies is well known. Early reports even proposed oscillatory

properties for ON1 (Wiese and Eilts, 1985), but low- and band-pass selectivity was also described—albeit by different measures (ISR: Nabatiyan et al., 2003, information rate: Marsat and Pollack, 2004). The observation of ON1's temporal tuning to the pulse rate of the conspecific calling song (Tunstall and Pollack, 2005) corroborates its role in a dedicated network and likely accounts for the firing-rate resonances observed here (fig. 4.5*C, F*).

In the high frequency channel the transfer functions of both ON1 and AN2 revealed temporal selectivity between 25 Hz and 40 Hz (fig. 4.5*B, C, E, F*; cf. Marsat and Pollack, 2004, 2005). Although burst coding of AN2 is known to mediate an evasive response in flying crickets (Marsat and Pollack, 2006), the firing-rate resonance within the frequency channel that is attributed to bat detection may also contribute to an adaptive response of flying crickets. For moths different evasive strategies upon bat detection are well known (Roeder, 1962) and may at least in part be mediated by a filter for high pulse rates (Boyan and Fullard, 1988). Upon target approach, a bat will typically increase the repetition rate of its echolocation calls from low rates of about 10 Hz to high rates of 200 Hz during the terminal buzz (Schnitzler and Kalko, 2001). Mantids utilize these temporal cues to initiate an appropriate diving response at about 20 Hz to 30 Hz (Triblehorn et al., 2008; Yager, 2012). Our results suggest that crickets may also exploit pulse rate cues to determine the distance from a predator. In this scenario, AN2 could play a role in mediating a tactical switch in the cricket's evasive behavior (Fullard et al., 2005).

4.4.3 Conclusion

I quantified firing-rate resonances in the early auditory system of *G. bimaculatus* by means of a novel protocol to record neuronal responses over a wide range of modulation frequencies. The protocol allowed for an efficient and robust collection of data and yielded commonly used measures for assessing a cell's processing of temporally patterned sounds. Most of the surveyed neurons expressed clear modulation tuning, indicating that—even in its periphery—the small nervous system of the cricket may focus its coding capacity on behaviorally-relevant cues.

5 From Neuronal Fundamentals to Firing-Rate Resonances

5.1 Introduction

For rhythmic signals that carry information in specific frequency bands, a neuronal system may profit from tuning its inherent filtering properties towards a peak sensitivity in the respective frequency range—especially if the system's size and computational resources are limited. In the previous two chapters, I examined individual neurons in the peripheral and higher auditory system of the cricket *G. bimaculatus* for tuning towards behaviorally relevant stimulus frequencies. Analysis of the experimental data revealed that—already in the periphery—some neurons indeed acted as tuned band-pass filters.

Female crickets recognize and selectively track the rhythmic calling songs of conspecific males (Popov et al., 1976). Due to the behavioral importance of these songs and their rhythmicity, an early specialization of peripheral neurons onto relevant frequency ranges may be an efficient computational strategy for this size-constrained network (Tunstall and Pollack, 2005). In the cricket's brain, several higher-order neurons have previously been found to respond selectively to acoustic stimuli that match the temporal features of the cricket's song (Schildberger, 1984; Zorović and Hedwig, 2011; Kostarakos and Hedwig, 2012). The sharpness of this tuning appears to increase from neuron to neuron in the sequence of processing (Schildberger, 1984; Zorović and Hedwig, 2011), hinting towards a distributed, cumulative filtering. The results from chapters 3 and 4 corroborate this idea and suggest that even neurons in the auditory periphery may contribute to such a filtering cascade.

The nature of the temporal filtering in the cricket's auditory system is still debated: proposed concepts include template matching (Hoy, 1978; Hennig, 2003), delay lines (Reiss, 1962; Weber and Thorson, 1989), subthreshold current oscillations (Eilts-Grimm and Wiese, 1984; Bush and Schul, 2006; Webb et al., 2007) and band-pass formation through interaction of low- and high-pass neu-

rons (Schildberger, 1984). Which mechanisms could be realized in the cricket's auditory periphery, given strict restraints on size and computational power?

Based on mathematical modeling, I implemented three very different mechanisms that can account for firing-rate resonances in small neuronal systems: (1) subthreshold resonance of the membrane impedance in single cells, (2) spike-triggered adaptation in single cells, and (3) networks with specific delays or frequency filtering. Despite differences in the underlying components, all of the mechanisms could faithfully reproduce the experimental findings of chapters 3 and 4. I discuss the relevance of the findings and hypothesize that a mixture of these mechanisms may shape responses to behaviorally relevant signals in the cricket's auditory periphery. I finally hypothesize that a serial combination of such filters could yield the strong tuning of auditory units in the cricket's brain.

5.2 Methods

This section only details methods specific to the present study. For a description of the more general methods involved, refer to chapter 2. See sections 4.2.1 and 4.2.2 for details on swept-frequency stimuli and the assessment of transfer functions.

5.2.1 Model 1: Resonate-and-Fire

To investigate the effects of membrane potential oscillations on a neuron's frequency transfer in the spiking regime, I adopted the Resonate-and-Fire model (as described in Erchova et al., 2004). The model's subthreshold dynamics correspond to the damped oscillations of an RLC circuit and are given by a two dimensional linear system:

$$C_\mathrm{m}\frac{\mathrm{d}}{\mathrm{d}t}V_\mathrm{m}(t) = I_\mathrm{in}(t) + I_\mathrm{n}(t) - I_\mathrm{lk}(t) - I_\mathrm{L}(t),$$
$$L\frac{\mathrm{d}}{\mathrm{d}t}I_\mathrm{L}(t) = V_\mathrm{m}(t) - V_0 - R_\mathrm{L}I_\mathrm{L}(t),$$

where

$$I_\mathrm{lk}(t) = \frac{1}{R_\mathrm{m}}(V_\mathrm{m}(t) - V_0).$$

The membrane potential V_m is diverted from its resting potential V_0 through injection of input current I_in and the presence of neuronal noise I_n. Depolarization is counteracted by both a leak current I_lk (governed by membrane resistance R_m and capacitance C_m) and an inductive current I_L. When V_m reaches a constant

threshold V_{th} an action potential is registered. V_m is then reset to a defined reset value V_r before the model progresses.

A subset of the model's parameters were fixed, with $V_0 = -70\,\text{mV}$, $V_{th} = -55\,\text{mV}$ and I_n resembling Gaussian white noise with a standard deviation of 100 pA. The amplitude of I_{in} was set to either 100 pA or 200 pA, resulting in sub- or suprathreshold voltage excursions, respectively. To approximate the rMTF of ON1, the model's remaining parameters were manually tuned to $V_r = -60\,\text{mV}$, $R_m = 143.0\,\text{M}\Omega$, $C_m = 54.6\,\text{pF}$, $L = 860\,\text{kH}$ and $R_L = 187.0\,\text{M}\Omega$. A detailed parameter scan was performed post hoc, illustrating the influence of inductance L and membrane time constant $\tau_m = R_m C_m$ on the model's frequency tuning. Simulations were performed at a temporal resolution of 200 µs. See table 5.1 for a summary of the model's parameters.

5.2.2 Model 2: Adaptive Leaky Integrate-and-Fire

The impact of spike-triggered adaptation and signal integration on a neuron's frequency response were explored by implementing an adaptive Leaky Integrate-and-Fire model (Treves, 1993). The subthreshold dynamics of the model are identical to the standard Leaky Integrate-and-Fire model and correspond to the characteristics of a low-pass RC circuit. They are given by

$$C_m \frac{\mathrm{d}}{\mathrm{d}t} V_m(t) = I_{in}(t) + I_n(t) - I_{lk}(t) - I_a(t).$$

In this model, a separate variable traces the progression of an adaptation current I_a which, by default, is zero. When the membrane potential crosses the firing threshold the adaptation variable is incremented by a predefined value ΔI_a and exponentially decays back to zero with time constant τ_a:

$$\tau_a \frac{\mathrm{d}}{\mathrm{d}t} I_a(t) = I_a(t).$$

The adaptation current I_a acts as a spike-dependent rectifier, driving V_m away from V_{th}.

For the model to approximate the rMTF of ON1, a subset of parameters was manually tuned to $V_r = -57\,\text{mV}$, $R_m = 59.0\,\text{M}\Omega$, $C_m = 59.6\,\text{pF}$, $\Delta I_a = 49.5\,\text{pA}$ and $\tau_a = 9.2\,\text{ms}$. The remaining parameters were identical to the ones used in the Resonate-and-Fire model. A subsequently applied parameter scan was used to illustrate the dependence of the model's frequency transfer on both the adaptation time constant τ_a and the membrane time constant τ_m. See table 5.1 for a summary of the model's parameters.

Table 5.1 Model Parameters: Spiking neuron models.

Parameter	Symbol	Value		Unit
		Model 1	Model 2	
Simulation rate	f_{s}	5	5	kHz
Resting potential	V_{m}	−70	−70	mV
Threshold potential	V_{th}	−55	−55	mV
Reset potential	V_{r}	−60	−57	mV
Membrane resistance	R_{m}	143.0	59.0	MΩ
Membrane capacitance	C_{m}	54.6	59.6	pF
Membrane time constant	τ_{m}	7.8	6.0	ms
Inductance	L	860	—	kH
Resistance (inductive branch)	R_{L}	187	—	MΩ
Adaptation time constant	τ_{a}	—	9.2	ms
Adaptation current increment	ΔI_{a}	—	49.5	pA
Input current (amplitude, subthreshold)	I_{in}	100	100	pA
Input current (amplitude, suprathreshold)	I_{in}	200	200	pA
Noise current[1] (mean)	$\mu_{I_{\mathrm{n}}}$	0	0	pA
Noise current[1] (standard deviation)	$\sigma_{I_{\mathrm{n}}}$	100	100	pA

[1] Gaussian white noise

5.2.3 Model 3: Linear-Nonlinear Network

A linear-nonlinear (LN) cascade (Schwartz et al., 2006; Clemens et al., 2012) was used to simulate the interactions of excitation and inhibition and their effect on frequency transfer in a small network:

$$r(t) = F[w_1(D_1 * s(t)) + w_2(D_2 * s(t - \Delta t))],$$

with

$$D_i * s(t) = \int_0^\infty D_i(\tau)\, s(t - \tau)\, \mathrm{d}\tau,$$

$$D_i(x) = \frac{1}{\sqrt{2\pi} \cdot \sigma_i} \cdot e^{-\frac{x^2}{2\sigma_i^2}}, \tag{5.1}$$

$$F(y) = \frac{a}{1 + e^{(y - y_0)b}}. \tag{5.2}$$

The model consisted of two branches, both of which acted as low-pass filters by convolving identical copies of an input signal $s(t)$ with a Gaussian kernel D of width σ. The corresponding cutoff frequencies were given by

$$f_{ci} = \sqrt{\ln 2} \cdot \frac{1}{2\pi\sigma_i}.$$

The output of the two branches was combined in a weighted sum, where one branch was assigned an excitatory ($w_1 > 0$) and the other one an inhibitory ($w_2 < 0$) role. Finally, a static nonlinearity F (a Boltzmann function with point of inflection y_0, saturation a, and width b) was applied, yielding a rectified spike-rate estimate r.

Taken alone, each branch acted as a causal low-pass filter. The system as a whole, however, can be equipped with band-pass properties by manipulating the branches in either the temporal or the spectral domain: In the first case (fig. 5.3), the model's two branches had identical low-pass properties ($\sigma_1 = \sigma_2$); the inhibitory branch, however, was given a delay $\Delta t > 0$. In the second case (fig. 5.4), the delay was omitted ($\Delta t = 0$). Instead, the cutoff frequency of the inhibitory low-pass filter was lowered relative to that of the excitatory branch ($\sigma_1 > \sigma_2$)[1].

The amplitude of stimulus $s(t)$ was set to 1. To achieve an approximation of ON1's rMTF through a delayed inhibition, the model's parameters were tuned to $\sigma_1 = \sigma_2 = 3\,\mathrm{ms}$, $w_1 = .88$, $w_1 = .12$, $\Delta t = 15\,\mathrm{ms}$, $y_0 = 0.75$, $a = 227\,\mathrm{Hz}$ and $b = 9$.

[1] Note: Because the model relies on *causal* filtering, lowering of a filters cut-off frequency effectively leads to an increased delay in the temporal domain.

Table 5.2 Model Parameters: Linear-Nonlinear network model.

			Value		
Segment	Parameter	Symbol	Model 3.1	Model 3.2	Unit
Input	Stimulus (amplitude)	s	1	1	—
Excitatory branch	Width of Gaussian[1]	σ_1	3.0	3.0	ms
	Cutoff frequency	f_{c1}	44.2	44.2	Hz
	Weight	w_1	0.88	0.84	—
Inhibitory branch	Width of Gaussian[1]	σ_2	3.0	6.5	ms
	Cutoff frequency	f_{c2}	44.2	20.4	Hz
	Delay	Δt	15	0	ms
	Weight	w_2	−0.12	−0.16	—
Nonlinearity[2]	Point of inflection	y_0	0.75	0.75	—
	Saturation	a	227	344	Hz
	Width	b	9	9	—

[1] Gaussian lowpass filter, see eq. 5.1
[2] Boltzmann function, see eq. 5.2

To reach the same objective through a spectral manipulation of the inhibitory component, parameters were tuned to $\sigma_1 = 3\,\text{ms}$, $\sigma_1 = 6.5\,\text{ms}$, $w_1 = .84$, $w_1 = .16$, $\Delta t = 0\,\text{ms}$, $y_0 = 0.75$, $a = 344\,\text{Hz}$ and $b = 9$. See table 5.2 for a comparison of the two models' parameters.

5.2.4 Pulse Response Arrays

After fitting the models to the modulation transfer of ON1, they were characterized by square wave stimulation. Inputs covered combinations of pulse and pause durations between 2.5 ms and 80 ms at a resolution of 2.5 ms. They had an average length corresponding to 1 s at the respective model's simulation rate. Transients were tapered by 1 ms ramps to mimic the envelope of the synthetic calling songs used in chapter 3. Responses of models 1 and 2 were averaged over 50 trials to increase the signal-to-noise ratio. Mean firing rates were presented as pulse response arrays (cf. section 3.2.3) to give a visualization of their dependance on pulse and pause durations. Cross sections of the pulse response arrays served to illustrate the responses to stimuli with constant pulse or pause durations (20 ms, respectively), constant duty cycle (0.5) and constant period (40 ms). The responses to symmetrical square-waves were contrasted with the responses to sine waves of equivalent fundamental frequencies.

5.2.5 Serial Combination of Models

To simulate a serial staging of identical filter elements, individual models were reiterated up to three times: each model's firing rate output was rescaled and then directly fed back to it as its input, ignoring the details of synaptic filtering. The only assumption that was made, was that each processing stage should receive the same peak input amplitude—that is, prior to each iteration, inputs were normalized to a maximum of 200 pA for models 1 and 2, and a maximum of 1 for models 3.1 and 3.2 (cf. tables 5.1 and 5.2). At each iteration level, filter properties were characterized by both the transfer function and the pulse response array (see section 5.2.4 for details).

Models 1 and 2 required additional processing in-between stages, as their discrete spiking output had to be translated to a continuous representation of firing rates. This was achieved by means of a KDE with a Gaussian kernel of width $\sigma = 2.5\,\mathrm{ms}$ (cf. section 2.6.2). The amplitude normalization between iterations was susceptible to noise, which affected the resolution of responses at higher iteration stages. To yield a sufficiently high signal-to-noise ratio, firing-rate estimates were averaged over 1000 repetitions.

5.3 Results

Results from my experiments suggested that both AN2 and ON1 reliably exhibit resonances within a behaviorally relevant frequency range (see chapter 4). In contrast to approaches like the ZAP protocol, which is used for the characterization of subthreshold frequency filtering (Gimbarzevsky et al., 1984), my experimental approach focussed on firing-rate resonances. Furthermore, the experiments were based on acoustic stimuli which did not drive the recorded cells directly. Instead, they were first processed by receptors and other neurons in the local network, so that the response characteristics were shaped both by the recorded neurons themselves and by upstream neurons. The observed resonances could hence be based on both cell-intrinsic and network-based mechanisms. Accordingly, I explored three simple and physiologically plausible models: (1) Subthreshold resonances, (2) spike-frequency adaptation, and (3) an interplay of excitation and inhibition. I tuned these models to match the average rMTF of ON1 (fig. 4.5*F*, $f_\mathrm{p} = 23.9\,\mathrm{Hz}$, $Q = 1.34$).

5.3.1 Subthreshold Resonances

In the first model, firing-rate resonances were induced cell-intrinsically through subthreshold resonances of the membrane potential. Subthreshold resonances

have been well characterized in many cell types (see Hutcheon and Yarom, 2000 for review) and give rise to band-pass filtering in the subthreshold range of membrane potentials. These filter properties can also carry over to the firing regime (Schreiber et al., 2004; Engel et al., 2008) and shape a firing-rate resonance (Richardson et al., 2003). I implemented a Resonate-and-Fire model (Erchova et al., 2004), where excursions of the membrane potential are counteracted by an inductive current. The model's resonant dynamics lead to an initial voltage overshoot in response to a subthreshold current pulse which translates into a corresponding overshoot of the firing rate in the suprathreshold regime (fig. 5.1*A, B*). Accordingly, resonances manifested themselves in both the sub- and suprathreshold frequency transfer (fig. 5.1*C, D*). By manually tuning the parameters (see table 5.1), the model displayed a firing-rate resonance at 23.9 Hz with a Q value of 1.34, closely resembling the rMTF of ON1. For frequencies above ~50 Hz, however, the model's frequency transfer diverged from the experimentally obtained data. For completeness, I note that this discrepancy stemmed from the limited number of model parameters, preventing an independent control of low- and high-frequency filter characteristics. The characteristics of the firing-rate resonance, like the peak frequency and Q value, depended on the model's parameters. To illustrate the robustness of tuning, these values are shown as a function of the parameters for inductance L and membrane time constant τ_{m} (fig. 5.1*E, F*). Both parameters correlated positively with the peak frequency and the Q value of the model's resonance, but to different degrees: While the membrane time constant had the bigger influence on the resonance's peak frequency, its Q value could be controlled by means of the inductance.

5.3.2 Spike-frequency Adaptation

The second model relies on the effect of adaptation, a universal phenomenon in neuronal systems that may be caused by a variety of mechanisms. Some of these mechanisms effectively depend on the occurrence of action potentials, as the adaptation currents are caused by ionic conductances that activate only at weakly negative or even positive membrane potentials which require large depolarizing voltage excursions. Such conductances can, for example, comprise M-type or mAHP-type currents with high activation thresholds (Benda and Herz, 2003). The adapting Leaky Integrate-and-Fire neuron (Treves, 1993) allows an implementation of an adaptation-based firing-rate resonance by combining high-pass properties of spike-triggered adaptation with low-pass properties of the non-resonant subthreshold voltage dynamics (fig. 5.2*A, B*). Here, the adaptation current only depended on the occurrence of spikes and, in contrast to

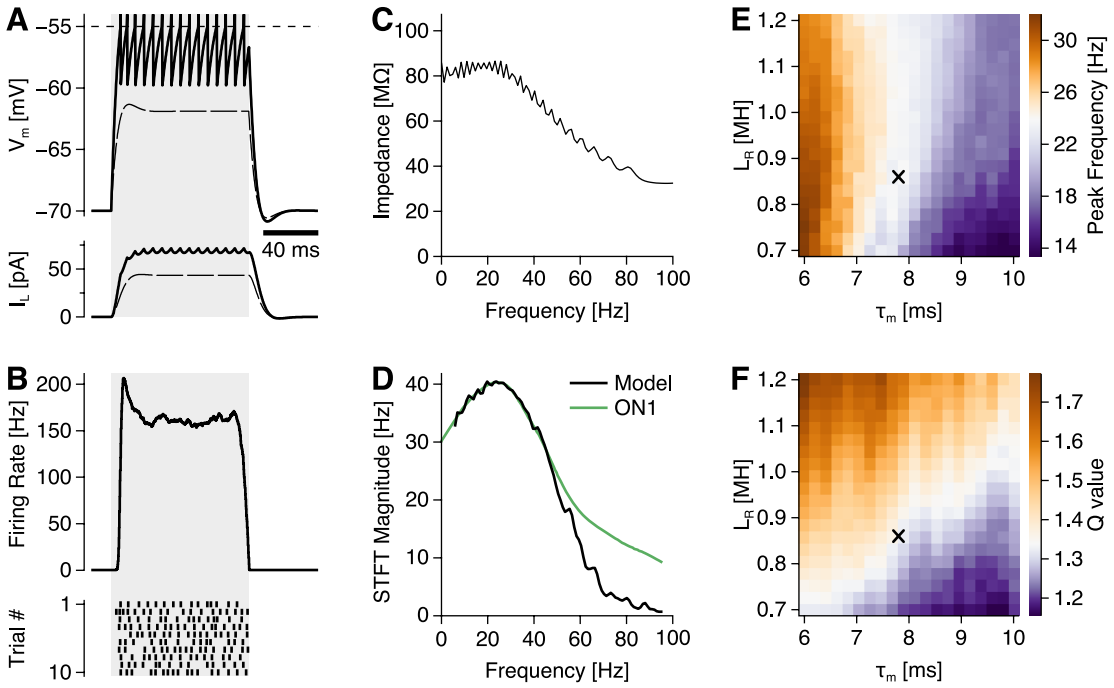

Figure 5.1 Model 1: Resonate-and-Fire. **A:** Subthreshold (dashed) and suprathreshold (solid) responses to current pulses of either 100 pA or 200 pA amplitude and 100 ms duration (gray). In this panel, the noise current was omitted for clarity. Note the damped oscillations during and after the pulse. **B:** Firing rate profile in response to a 200 pA pulse, 20 repetitions. Instantaneous spike rate (top) and exemplary spike raster plot (bottom). **C:** The subthreshold impedance amplitude profile (ZAP) displayed a weak resonance peak at 19.3 Hz with a Q value of 1.04. **D:** Suprathreshold frequency transfer, 50 repetitions, peaking at 23.9 Hz with a Q value of 1.34. **E, F:** A parameter scan serves to illustrate the impact of membrane time constant τ_{m} and inductance L on peak frequency and Q value. The parameter combination used in **A–D** is marked by a cross.

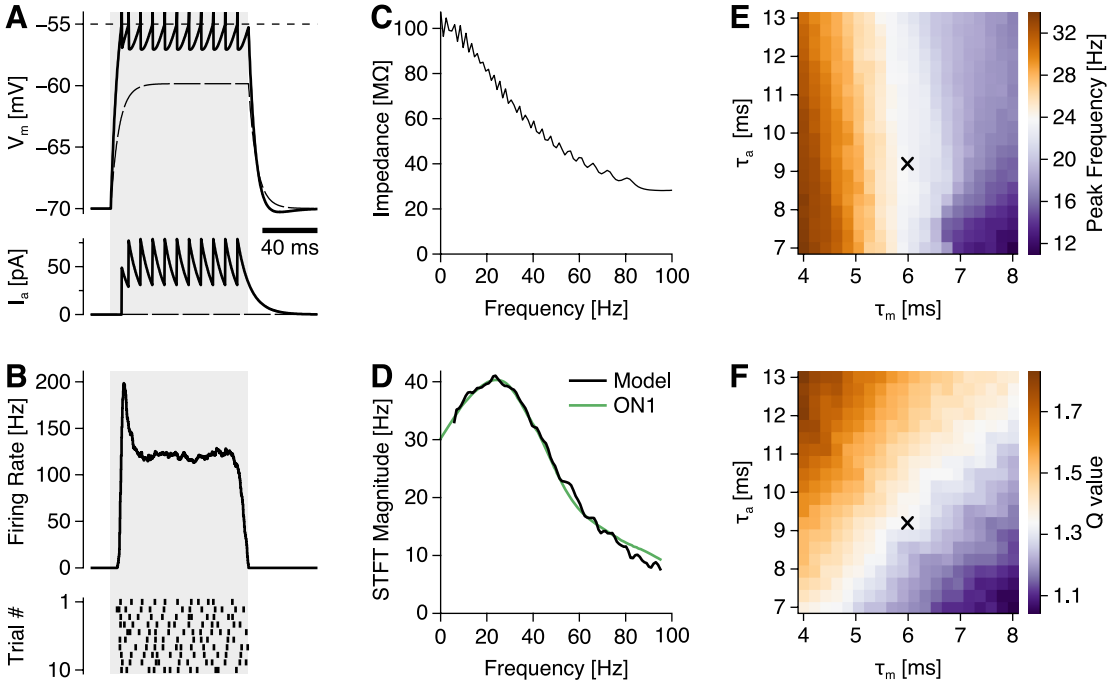

Figure 5.2 Model 2: adapting Leaky Integrate-and-Fire. **A:** Subthreshold (dashed) and suprathreshold (solid) responses to current pulses of either 100 pA or 200 pA amplitude and 100 ms duration (gray). In this panel, the noise current was omitted for clarity. The adaptation current I_a is increased with each spike and decays in an exponential manner. **B:** Firing rate profile in response to a 200 pA pulse with added noise current, 20 repetitions. Instantaneous spike rate (top) and exemplary spike raster plot (bottom). **C:** The subthreshold impedance amplitude profile (ZAP) displayed no resonance. **D:** Suprathreshold frequency transfer, 50 repetitions, peaking at 23.6 Hz with a Q value of 1.34. **E, F:** A parameter scan serves to illustrate the impact of membrane time constant τ_m and adaptation time constant τ_a on peak frequency and Q value. The parameter combination used in **A–D** is marked by a cross.

the model described above, the voltage dynamics did not exhibit band-pass properties in the subthreshold regime (fig. 5.2*C*). In the spiking regime, however, the adaptation current I_a added a high-pass component to the response, leading to a firing-rate resonance (fig. 5.2*D*).

By tuning the model's parameters I was able to obtain a peak frequency of 23.6 Hz with a Q value of 1.34, closely matching the data obtained for ON1. I again applied anexemplar parameter scan to illustrate the influence of individual model parameters on the characteristics of the resonance. While the peak frequency of the resonance was strongly influenced by the membrane time constant τ_m, the adaptation time constant τ_a had only little effect (fig. 5.2*E*). Nevertheless, τ_a exhibited a clear influence on the Q value of the firing-rate resonance (fig. 5.2*F*).

5.3.3 Interplay of Excitation and Inhibition

Computation within the cricket's auditory system is not limited to intracellular mechanisms. Despite its small size, the prothoracic system has an interesting topology that includes both excitatory and inhibitory elements (Wohlers and Huber, 1982). ON1 neurons, in particular, receive excitatory inputs from the receptor populations and inhibitory inputs from their contralateral counterpart. I hence implemented a simple model of the local network based on a linear-nonlinear (LN) cascade and investigated the formation of firing-rate resonances based on the interactions of excitatory and inhibitory network components. Specifically, I analyzed two versions of the model, equivalent to different physiological implementations. Both provide a firing rate estimate by computing the weighted sum of two low-pass filtered copies of the stimulus—one of them "excitatory" (additive), the other one "inhibitory" (subtractive)—and applying a rectifying Boltzmann non-linearity (figs. 5.3 and 5.4). Resonances were introduced through parameters of the inhibition – either in time or in the frequency domain. In the first case, a temporal delay Δt was added to the inhibitory branch (fig. 5.3*A*). While this did not affect the two branches' individual frequency transfers (fig. 5.3*C*), their combined output showed a clear resonance which I tuned to a peak frequency of 23.8 Hz and a Q value of 1.35 (fig. 5.3*D*). In the second case, the low-pass filter of the inhibitory branch was set to a lower cutoff frequency than that of the excitatory branch (fig. 5.4*A*). After tuning the respective parameters (see table 5.1), the two filters' frequency transfers (fig. 5.4*C*) combined to an accurate approximation of the rMTF of ON1, with a peak frequency of 23.8 Hz and a Q value of 1.37.

5.3.4 Pulse Response Arrays

The four models yielded almost identical responses to square-wave inputs (fig. 5.5E_i–H_i and fig. 5.6*B*), resembling the strong duty cycle dependence of ON1 (cf. fig. 3.2*H, I*). Across pulse periods, symmetrical square-wave inputs yielded steady response rates which only dropped off for periods below 40 ms (fig. 5.6*A*). The Resonate-and-Fire model stood out, as it consistently produced stronger responses to high DC square-waves than the other models (fig. 5.6*A*-*D*). This was also reflected in the model's comparatively high steady state pulse response (fig. 5.1*B*). Square-wave responses were generally about 20–25 Hz higher in rate than the responses to sine-wave inputs of equal periods (fig. 5.6*A*). Furthermore, they lacked the slight drop-off towards long periods (i.e., low modulation frequencies) apparent in sine-wave responses.

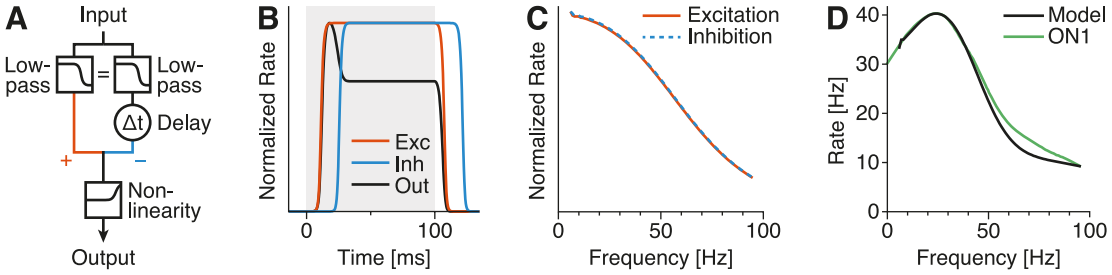

Figure 5.3 Model 3.1: LN Network, variant 1. **A:** Schematic. The input was processed in two parallel branches, one excitatory (+) and one inhibitory (−). In both branches, the signal was low-pass filtered with identical cutoff frequencies. In the inhibitory branch, however, the signal was delayed by Δt. The weighted sum of the two branches' output was passed through a sigmoidal non-linearity to obtain a firing rate estimate. **B:** Response of the model and its components to a pulse stimulus (gray). Note the onset peak of the model's output. **C:** Identical frequency transfer of the model's excitatory and inhibitory branches. **D:** Frequency transfer of the model compared to data measured during experiments.

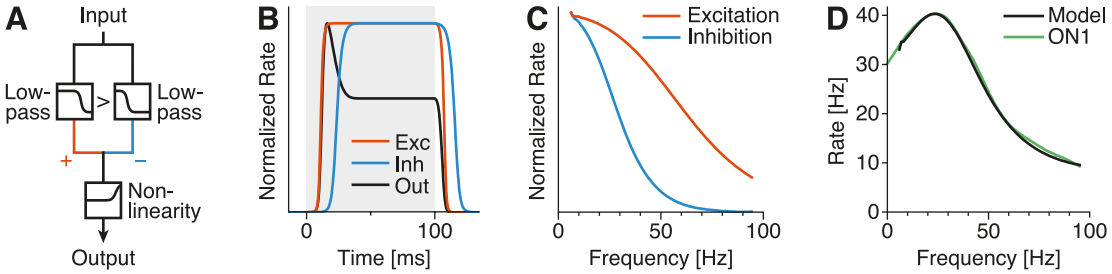

Figure 5.4 Model 3.2: LN Network, variant 2. **A:** Schematic. Like in the previous model, the input is simultaneously processed by an excitatory (+) and an inhibitory (-) branch, both of which acted as low-pass filters. The cutoff frequency of the inhibitory branch was lower than that of the excitatory branch. The weighted sum of the two branches' output was passed through a sigmoidal non-linearity to obtain a firing rate estimate. **B:** Response of the model and its components to a pulse stimulus (gray). **C:** Frequency transfer of the model's excitatory and inhibitory branches. **D:** Frequency transfer of the model compared to data measured during experiments.

5.3.5 Serial Combination of Models

To simulate a serial staging of individual filter elements, the models' output was repeatedly rescaled and fed back as an input to the model. Iterating over individual models consistently yielded a decrease in response rates and a sharpening of their temporal tuning. This was apparent in both the model's transfer functions derived from sine-wave inputs (fig. 5.5*A–D*) and their pulse response arrays derived from square-wave inputs (fig. 5.5*E–H*). Already at the second iteration stage, models showed a strong preference for pulse durations between 20 ms and 30 ms and pause durations of 10 ms to 20 ms (fig. 5.5E_{ii}–H_{ii}). At the third iteration stage, the sharpness of tuning increased further, while firing rates dropped to very low levels (figs. 5.5 and 5.5E_{iii}–H_{iii}). Model 2 virtually ceased firing altogether (fig. 5.5F_{iii}). Furthermore, with each iteration, transfer functions of all models shifted towards slightly lower peak frequencies (fig. 5.5*A–D*).

5.4 Discussion

5.4.1 Reproduction of Experimental Data by Different Models

Three different models, based on either cell-intrinsic or network based mechanisms, could be fitted to match the experimentally observed firing-rate resonances of ON1 (cf. chapter 4). In the first model—an implementation of the Resonate-and-Fire model by Erchova et al. (2004)—firing-rate resonances emerged from a band-pass in the subthreshold membrane impedance (fig. 5.1). Webb et al. (2007) demonstrated that such a mechanism could explain phonotactic preference functions of bushcrickets by fitting a similar model (Izhikevich, 2001) to behavioral data of *Tettigonia cantans*. Subthreshold resonances did not have to be particularly strong—a subthreshold Q value of 1.04 was sufficient to yield the experimentally observed firing-rate resonance (fig. 5.1*C*). Whether this mechanism is in fact realized in the cricket's auditory periphery could be ascertained by means of intracellular recordings and the ZAP protocol. Previous studies involving intracellular recordings, however, did not give any indications for subthreshold resonances (Wohlers and Huber, 1978, 1982; Selverston et al., 1985).

In the second model, a variation of the Leaky Integrate-and-Fire model, subthreshold voltage dynamics were nonresonant (fig. 5.2). In the suprathreshold regime, however, a spike-triggered, slowly decaying adaptation current provided suppression of low frequencies (Benda and Hennig, 2008). As in the first model, parameters affected different aspects of the resonance, enabling us to independently tune peak frequency and Q value (fig. 5.2*E*, *F*). The resonance-generating mechanism is very similar to the Resonate-and-Fire model: Potassium channels,

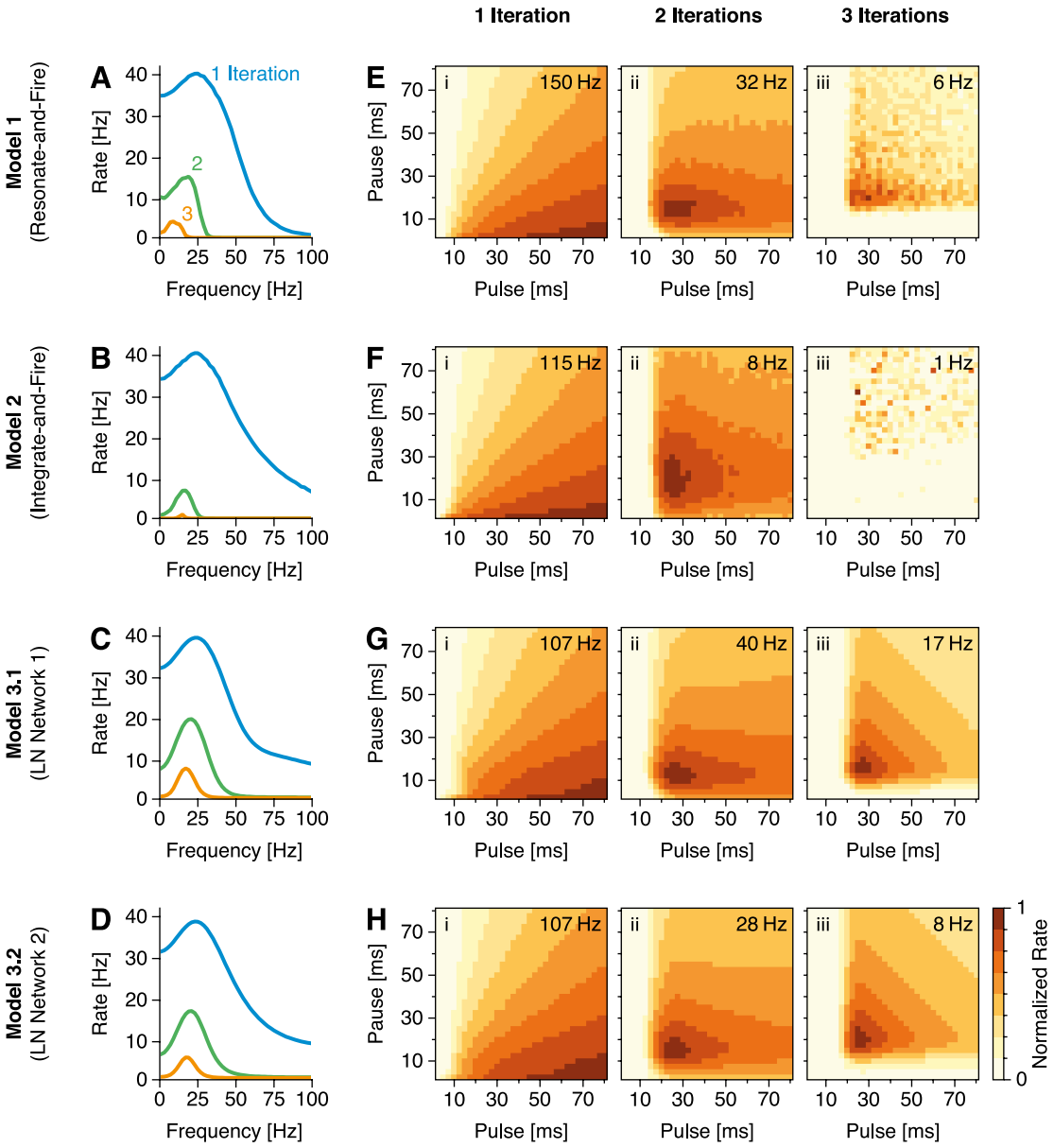

Figure 5.5 Serial Combination of Models. To simulate a serial staging of identical filter elements, each model's firing rate output was fed back to it as its input. Individual models were reiterated up to three times. Responses during the first iteration correspond to those of the original models (cf. figs. 5.1 to 5.4). **A–D:** Transfer functions obtained through stimulation with sine waves. **E–H:** Pulse response arrays obtained through stimulation with square waves. Maximum response rates are indicated in the top right corner of each panel.

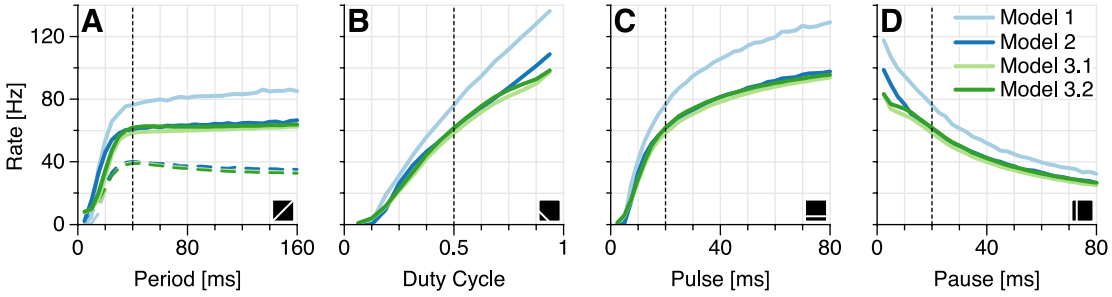

Figure 5.6 Cross sections of the pulse response arrays (cf. fig. 5.5E_i–H_i). Dotted lines mark the song parameters of *G. bimaculatus*, pictograms indicate the cross sections' orientation within the parameter space. **A:** Constant duty cycle (0.5). Dashed lines indicate responses to sine-wave stimuli. **B:** Constant period (40 ms). **C:** Constant pulse duration (20 ms). **D:** Constant pause duration (20 ms).

for instance, could underlie the resonances in both models, but their activation curves would be shifted. For activation of potassium channels at lower voltages, a subthreshold resonance becomes evident. If, however, the potassium channel activation curve is shifted towards more depolarized voltages (so that activation is only achieved during APs), resonance manifests itself only in the supra-, but not the subthreshold range. Subthreshold resonance and spike-frequency adaptation are thus mechanistically and biophysically highly related phenomena.

In the third model, band-pass filtering relied on the combination of low-pass excitation and low-pass inhibition in a network of linear-nonlinear (LN) neurons. In one version of the model, high-pass properties were introduced by a temporal delay in the network's inhibitory branch: Input components shorter than this delay fully contributed to the rectified output rate; longer ones were attenuated by inhibition (fig. 5.3). In an alternative version of the model, band-pass filtering arose from differences in the spectral structure of the excitatory and inhibitory signal (fig. 5.4). Inhibition specifically reduced low frequency components of a more broadly-tuned excitation. Both versions of the model yielded a faithful reproduction of the experimentally obtained firing-rate resonance. Nevertheless, in the first version of the model delays on the order of ~15 ms were needed. Such large delays seem unlikely for a system as small as the cricket's prothoracic auditory network. The model based on the subtractive combination of low-pass filters with different cutoff frequencies seems more plausible in this context.

5.4.2 Exploration of New Parameter Spaces

After fitting the models to the modulation transfer characteristics of ON1, they were exposed to square-wave inputs that mimicked the artificial calling songs

used in chapter 3. While the pulse response array of ON1 built on stimuli with a carrier frequency of 4.5 kHz, models were fitted to ON1's rMTF at a carrier frequency of 16 kHz, precluding a detailed comparison. Nevertheless, all four models readily reproduced the general characteristics of ON1's pulse response arrays (fig. 3.2), as their firing-rates strongly depended on the stimuli's duty cycle (fig. 5.5E_i–H_i and fig. 5.6*B*). The models thus also held for extended parameter spaces which they had not been exposed to during the initial parameter fitting.

The comparison of square-wave and sine-wave inputs confirmed that the latter are better suited for characterizing a system's frequency transfer: The faint high-pass components of the four models' transfer functions were only discernable in responses to sine-wave inputs (fig. 5.6*A*). For square-wave signals, the attenuation of low frequencies was apparently masked by the ever-present high-frequency harmonics—that is, by the consistently strong responses to the steep pulse onsets, which are unaffected by changes in pulse rate. This could explain why the bandpass tuning of ON1 was not apparent in the pulse response arrays (fig. 3.2*H*), but only in the MTFs deduced from SFAM stimuli (fig. 4.5*C*).

The serial combination of models quickly led to a sharpening of tuning and an overall decrease in response rates (fig. 5.5). This corroborates findings for brain neurons, as these show a similar progression of physiological properties (fig. 3.7; Schildberger, 1984; Zorović and Hedwig, 2011; Kostarakos and Hedwig, 2012). The filtering observed for ON1 and AN2 could thus be a general motif across the cricket's auditory system: a serial combination of similar or identical weak filters could yield the strong filtering observed in brain neurons *en passant*, that is, without the need for a *dedicated* filter element. Such a repetitive exploitation of pervasive mechanisms could be a parsimonious adaptation to the constraints of a small neuronal system. It could entail beneficial effects on several levels, including size, computational and genetic complexity, as well as energy budget.

For a serial combination of *identical* filter elements, intracellular mechanisms seem the most plausible candidates, as they do not require specialized connectivity. For the cricket, however, even a cascade of network based filters seems conceivable, as inhibitory inputs are present throughout its auditory system (prothoracic neurons: Selverston et al., 1985; Horseman and Huber, 1994a; brain: Kostarakos and Hedwig, 2012). Ultimately, the cascade could also comprise a mixture of different filtering implementations, although this would add additional complexity.

5.4.3 Conclusion

The different models illustrate that several mechanisms can produce bandpass properties: Subthreshold resonances, spike-triggered adaptation, as well as

the interplay of excitation and inhibition. All four models share a delayed negative feedback component, implemented either through ion channels (for the single-cell models) or at the level of synaptic transmission (for the network models). The resonance observed in the experimental data could be produced by the interplay of several of these mechanisms – future studies will identify the contribution of individual mechanisms by quantifying the subthreshold impedance, firing rate adaptation, or the timing of inhibitory versus excitatory inputs. The resonances observed in the prothoracic auditory system are possibly part of a distributed filtering cascade: Several serially arranged filter elements of moderate strength could accumulate to produce the strong pulse rate preference seen in both auditory brain neurons (Schildberger, 1984; Zorović and Hedwig, 2011; Kostarakos and Hedwig, 2012) and behavior (Hennig, 2009). Such a strategy could be a beneficial adaptation for processing sound in a highly specialized, size-constrained auditory system.

6 Conclusion

The objective of this work was to investigate neuronal adaptations for signal processing in size-constrained, specialized sensory systems. I examined individual neurons in the auditory system of the cricket, *G. bimaculatus*, as to specific tuning towards behaviorally relevant stimulus parameters. To do so, I pursued a classical black box approach: By combining acoustic stimulation with extracellular electrophysiology, I assessed the transfer characteristics of neurons throughout the cricket's auditory system. I then explored several feasible system implementations by means of mathematical modelling.

Using square-wave modulated stimuli, I obtained detailed response profiles of both prothoracic and higher-level auditory neurons (chapter 3). The results suggested that even peripheral auditory neurons may be adaptapted towards the temporal features of conspecific signals. To follow up on these findings, I obtained the modulation transfer functions of prothoracic auditory units by means of an effective, novel stimulation paradigm (chapter 4). The results corroborated those of the previous chapter, as most of the surveyed neurons expressed clear firing-rate resonances that matched the modulation characteristics of the male cricket's song. In the next step, I tried to infer plausible filtering mechanisms that could implement the experimental findings: I used simple computational models that based on common, cell-intrinsic or network-based mechanisms and tuned them to match the experimentally observed firing-rate resonances (chapter 5). These mechanisms included subthreshold resonances, spike-triggered adaptation, as well as the interplay of excitation and inhibition. I finally showed how a serial combination of such elementary filters could yield the strong selectivity evident in the cricket's behavior.

In conclusion, my work should convey that (1) peripheral filtering can be a beneficial adaptation towards the efficient processing of signals in a specialist sensory system; (2) common, cell-intrinsic or network-based mechanisms can yield articulate firing-rate resonances; and (3) a serial combination of elementary filters could constitute a filtering-cascade, offering strong and efficient tuning to relevant signal components.

The proposed mechanisms constitute elementary building blocks of neuronal signal processing and are thus easily transferable to other, more complex sensory systems. The presented work encourages future studies that will further elucidate the role of neuronal adaptations towards efficient sensory processing. Intracellular recording techniques will help in narrowing down the implementation of the observed firing-rate resonces and will be pertinent in assessing the relevance of sequential filtering cascades.

Danksagung

Mein erster Dank gilt **Matthias Hennig** für die Betreuung meiner Arbeit. Er war stets sorgfältig, fair und aufrichtig, hatte einen Blick fürs Detail und ein Gespür für Problemstellen. Ich habe viel gelernt! **Susanne Schreiber** danke ich für die gelungene Kooperation, zahllose Diskussionen sowie die vorbehaltlose und großzügige Unterstützung meiner Arbeit. Ich danke **Martin Nawrot** für den ursprünglichen Impuls, mich in Berlin den Grillen zu widmen, für fachliche und persönliche Diskussionen sowie für die überaus gelungenen Tagungen mit seiner Arbeitsgruppe. **Bernhard Ronacher** danke ich für Ratschläge und Kritik, sowie für die Möglichkeit, Teil seiner Arbeitsgruppe zu sein.

Ich danke all jenen, die unmittelbar zur Entstehung dieser Doktorarbeit beigetragen haben: **Jan Clemens** für Modellierungsansätze, kritische Diskussionen und zahllose Tipps; **Victor Naumov** für saubere Konnektivableitungen; **Regina Lübke** für Aufzucht und Pflege der Tiere; **Nicole Stange** für Hilfe in Sachen Statistik; **Jan-Hendrik Schleimer** und **Frederic Römschied** für hilfreiche Diskussionen und Literaturhinweise; **Michael Reichert** und **Vanessa Stempel** für unermüdliches Korrekturlesen; sowie **Manuel Gersbacher** für detaillierte Kritik meiner Abbildungen.

In der *VhPhys* sind die Grenzen zwischen AG und WG bis zur Unkenntlichkeit verwischt. Tatsächlich habe ich mich hier stets zuhause gefühlt. Mein besonderer Dank gilt daher meinen „Mitbewohnern“, die dies ermöglicht haben: **Jan** für Cocktails, Kätzchen und Drum & Bass; **Jannis** für Starthilfe in Sachen Grillen, Volleyball und Kickern; **Nic** für morgendliche Kaffeeverlockungen, sowie Stadtteiltouren zu Tag und zu Nacht; **Olaf** für Fluppen, Nachtschichten im Nemo und ungezügelte Stimmung; **Daniela** für Musik, Rum Bars und eine tolle Wohnung; **Sarah** für gemeinsames Pöbeln, Lästern und Salmiakkigelüste; **Jonas** für Croissants, verbeulte Bleche und ein allzeit freies Sofa; **Fred** für Integrale, Fresschen und Kickern bis et kracht; **Arnulf** für Konzerte, Third Wave Coffee und italienische Prachtkompositionen; **Moni** für forcierte Kaffeepausen und Vogelkunde; **Michael** für Hilfslieferungen aus den USA und *hot sauce mayhems*; **Fabian** für Fotofachsimpeleien und gute Gespräche; **Victor** für die weltbesten

Hakenelektroden und russisches Liedgut; **Matti** für Hip-Hop, Tags und fleißiges Ableiten; **Gundula** für Mathematik, Bibimbap und Fahrradkunde; **Fleur** für räumliche Orientierung und großartige Spätzle; sowie **Stef** für die heimelige Terrassenbegrünung. **Eileen** und **Thomas** wünsche ich das Beste für die Arbeit mit den Grillen – haltet die Fahne hoch! **Jenny**, hab einen guten Start in der AG Verhaltensphysiologie!

Mein besonderer Dank gilt meinen **Eltern**, meinen **Freunden** sowie **Susanne**. Für Unterstützung, Geduld und jede einzelne Minute jenseits der Wissenschaft.

Bibliography

Atkins G, Henley J, Handysides R, Stout J (1992) Evaluation of the behavioral roles of ascending auditory interneurons in calling song phonotaxis by the female cricket (*Acheta domesticus*). J Comp Physiol [A] 170:363–72.

Atkins G, Ligman S, Burghardt F, Stout JF (1984) Changes in phonotaxis by the female cricket *Acheta domesticus* L. after killing identified acoustic interneurons. J Comp Physiol [A] 154:795–804.

Atkins G, Pollack GS (1986) Age-dependent occurrence of an ascending axon on the omega neuron of the cricket, *Teleogryllus oceanicus*. J Comp Neurol 243:527–34.

Barlow HB (1961) Possible principles underlying the transformation of sensory messages. In: Sensory communication (Rosenblith WA, ed), pp 217–34. Cambridge: MIT Press.

Benda J, Hennig RM (2008) Spike-frequency adaptation generates intensity invariance in a primary auditory interneuron. J Comput Neurosci 24:113–36.

Benda J, Herz AVM (2003) A universal model for spike-frequency adaptation. Neural Comput 15:2523–64.

Bennet-Clark HC (1989) Songs and the physics of sound production. In: Cricket behavior and neurobiology (Huber F, Moore TE, Loher W, eds), pp 227–61. Ithaca: Cornell UP.

Bessou P, Laporte Y, Pagés B (1968) A method of analysing the responses of spindle primary endings to fusimotor stimulation. J Physiol 196:37–45.

Blatt M, Wiseman S, Domany E (1996) Superparamagnetic clustering of data. Phys Rev Lett 76:3251–54.

Borst A, Theunissen FE (1999) Information theory and neural coding. Nat Neurosci 2:947–57.

Boyan GS, Fullard JH (1988) Information processing at a central synapse suggests a noise filter in the auditory pathway of the noctuid moth. J Comp Physiol [A] 164:251–58.

Boyan GS, Williams JLD (1982) Auditory neurones in the brain of the cricket *Gryllus bimaculatus* (De Geer): Ascending interneurones. J Insect Physiol 28:493–501.

Bush SL, Schul J (2006) Pulse-rate recognition in an insect: Evidence of a role for oscillatory neurons. J Comp Physiol [A] 192:113–21.

Cariani PA (2001) Specialist and generalist strategies in sensory evolution. Artif Life 7:211–14.

Clemens J, Kutzki O, Ronacher B, Schreiber S, Wohlgemuth S (2011) Efficient transformation of an auditory population code in a small sensory system. Proc Natl Acad Sci USA 108:13812–17.

Clemens J, Wohlgemuth S, Ronacher B (2012) Nonlinear computations underlying temporal and population sparseness in the auditory system of the grasshopper. J Neurosci 32:10053–62.

Doherty JA (1985) Temperature coupling and 'trade-off' phenomena in the acoustic communication system of the cricket, *Gryllus bimaculatus* De Geer (Gryllidae). J Exp Biol 114:17–35.

Eggermont JJ, Wang X (2011) Temporal coding in auditory cortex. In: The Auditory Cortex (Winer JA, Schreiner CE, eds), pp 309–28. New York: Springer.

Eilts-Grimm K, Wiese K (1984) An electrical analogue model for frequency dependent lateral inhibition refering to the omega neurons in the auditory pathway of the cricket. Biol Cybern 51:45–52.

Engel TA, Schimansky-Geier L, Herz AVM, Schreiber S, Erchova I (2008) Subthreshold membrane-potential resonances shape spike-train patterns in the entorhinal cortex. J Neurophysiol 100:1576–89.

Erchova I, Kreck G, Heinemann U, Herz AVM (2004) Dynamics of rat entorhinal cortex layer II and III cells: Characteristics of membrane potential resonance at rest predict oscillation properties near threshold. J Physiol 560:89–110.

Farris H, Mason A, Hoy RR (2004) Identified auditory neurons in the cricket *Gryllus rubens*: Temporal processing in calling song sensitive units. Hear Res 193:121–33.

Faulkes Z, Pollack G (2001) Mechanisms of frequency-specific responses of omega neuron 1 in crickets (*Teleogryllus oceanicus*): A polysynaptic pathway for song? J Exp Biol 204:1295–305.

Faulkes Z, Pollack GS (2000) Effects of inhibitory timing on contrast enhancement in auditory circuits in crickets (*Teleogryllus oceanicus*). J Neurophysiol 84:1247–55.

Fettiplace R (1987) Electrical tuning of hair cells in the inner ear. Trends Neurosci 10:421–25.

Fullard JH, Ratcliffe JM, Guignion C (2005) Sensory ecology of predator-prey interactions: Responses of the AN2 interneuron in the field cricket, *Teleogryllus oceanicus* to the echolocation calls of sympatric bats. J Comp Physiol [A] 191:605–18.

Gade S, Herlufsen H (1987) Use of weighting functions in DFT/FFT analysis (Part I). Brüel & Kjær Technical Review 3:1–28.

Gerstein GL, Kiang NY (1960) An approach to the quantitative analysis of electrophysiological data from single neurons. Biophys J 1:15–28.

Gerstner W, Kreiter AK, Markram H, Herz AV (1997) Neural codes: Firing rates and beyond. Proc Natl Acad Sci USA 94:12740–41.

Gimbarzevsky B, Miura RM, Puil E (1984) Impedance profiles of peripheral and central neurons. Can J Physiol Pharmacol 62:460–62.

Goertzel G (1958) An algorithm for the evaluation of finite trigonometric series. Am Math Mon 65:34–35.

Gold C, Henze DA, Koch C, Buzsáki G (2006) On the origin of the extracellular action potential waveform: A modeling study. J Neurophysiol 95:3113–28.

Gray DA, Cade WH (2000) Sexual selection and speciation in field crickets. Proc Natl Acad Sci USA 97:14449–54.

Grobe B, Rothbart MM, Hanschke A, Hennig RM (2012) Auditory processing at two time scales by the cricket (*Gryllus bimaculatus*). J Exp Biol 215:1681–90.

Gross CG, Bender DB, Rocha-Miranda CE (1969) Visual receptive fields of neurons in inferotemporal cortex of the monkey. Science 166:1303–6.

Haar A (1910) Zur Theorie der orthogonalen Funktionensysteme. Math Ann 69:331–71.

Heil P (2004) First-spike latency of auditory neurons revisited. Curr Opin Neurobiol 14:461–67.

Hennig RM (1988) Ascending auditory interneurons in the cricket *Teleogryllus commodus* (Walker): Comparative physiology and direct connections with afferents. J Comp Physiol [A] 163:135–43.

Hennig RM (2003) Acoustic feature extraction by cross-correlation in crickets? J Comp Physiol [A] 189:589–98.

Hennig RM (2009) Walking in Fourier's space: Algorithms for the computation of periodicities in song patterns by the cricket *Gryllus bimaculatus*. J Comp Physiol [A] 195:971–87.

Hennig RM, Franz A, Stumpner A (2004) Processing of auditory information in insects. Microsc Res Tech 63:351–74.

Hildebrandt KJ (2014) Neural maps in insect versus vertebrate auditory systems. Curr Opin Neurobiol 24:82–87.

Hodgkin AL (1954) A note on conduction velocity. J Physiol 125:221–24.

Horseman G, Huber F (1994a) Sound localisation in crickets. I. Contralateral inhibition of an ascending auditory interneurone. J Comp Physiol [A] 175:389–98.

Horseman G, Huber F (1994b) Sound localisation in crickets. II. Modelling the role of a simple neural network in the prothoracic ganglion. J Comp Physiol [A] 175:399–413.

Hoy RR (1978) Acoustic communication in crickets: A model system for the study of feature detection. Fed Proc 37:2316–23.

Hubel DH, Wiesel TN (1962) Receptive fields, binocular interaction and functional architecture in the cat's visual cortex. J Physiol 160:106–54.

Hubel DH, Wiesel TN (1968) Receptive fields and functional architecture of monkey striate cortex. J Physiol 195:215–43.

Huber F, Moore TE, Loher W (eds) (1989) Cricket behavior and neurobiology. Ithaca: Cornell UP.

Huber F, Thorson J (1985) Cricket auditory communication. Sci Amer 253:46–54.

Hutcheon B, Yarom Y (2000) Resonance, oscillation and the intrinsic frequency preferences of neurons. Trends Neurosci 23:216–22.

Imaizumi K, Pollack GS (2001) Neural representation of sound amplitude by functionally different auditory receptors in crickets. J Acoust Soc Am 109:1247–60.

Izhikevich EM (2001) Resonate-and-fire neurons. Neural Netw 14:883–94.

Katz B, Miledi R (1965a) The effect of temperature on the synaptic delay at the neuromuscular junction. J Physiol 181:656–70.

Katz B, Miledi R (1965b) The measurement of synaptic delay, and the time course of acetylcholine release at the neuromuscular junction. Proc R Soc Lond B Biol Sci 161:483–95.

Koch C (1984) Cable theory in neurons with active, linearized membranes. Biol Cybern 50:15–33.

Kostarakos K, Hedwig B (2012) Calling song recognition in female crickets: Temporal tuning of identified brain neurons matches behavior. J Neurosci 32:9601–12.

Kramer E (1976) The orientation of walking honeybees in odour fields with small concentration gradients. Physiol Entomol 1:27–37.

Kuffler SW (1953) Discharge patterns and functional organization of mammalian retina. J Neurophysiol 16:37–68.

MacQueen J (1967) Some methods for classification and analysis of multivariate observations. In: Proceedings of the fifth Berkeley symposium on mathematical statistics and probability, volume 1, pp 281–97. Berkeley: University of California Press.

Malone B, Schreiner CE (2010) Time-varying sounds: Amplitude envelope modulations. In: The Oxford Handbook of Auditory Science: The Auditory Brain (Rees A, Palmer AR, eds), pp 125–48. Oxford: Oxford UP.

Marsat G, Pollack GS (2004) Differential temporal coding of rhythmically diverse acoustic signals by a single interneuron. J Neurophysiol 92:939–48.

Marsat G, Pollack GS (2005) Effect of the temporal pattern of contralateral inhibition on sound localization cues. J Neurosci 25:6137–44.

Marsat G, Pollack GS (2006) A behavioral role for feature detection by sensory bursts. J Neurosci 26:10542–47.

Meckenhäuser G, Hennig RM, Nawrot MP (2013) Critical song features for auditory pattern recognition in crickets. PLoS One 8:e55349.

Moiseff A, Pollack GS, Hoy RR (1978) Steering responses of flying crickets to sound and ultrasound: Mate attraction and predator avoidance. Proc Natl Acad Sci USA 75:4052–56.

Nabatiyan A, Poulet JFA, de Polavieja GG, Hedwig B (2003) Temporal pattern recognition based on instantaneous spike rate coding in a simple auditory system. J Neurophysiol 90:2484–93.

Nawrot M, Aertsen A, Rotter S (1999) Single-trial estimation of neuronal firing rates: From single-neuron spike trains to population activity. J Neurosci Methods 94:81–92.

Nawrot MP, Boucsein C, Rodriguez Molina V, Riehle A, Aertsen A, Rotter S (2008) Measurement of variability dynamics in cortical spike trains. J Neurosci Methods 169:374–90.

Nolen TG, Hoy RR (1984) Initiation of behavior by single neurons: The role of behavioral context. Science 226:992–94.

Ostrowski TD, Stumpner A (2014) Response differences of intersegmental auditory neurons recorded close to or far away from the presumed spike-generating zone. J Comp Physiol [A] 200:627–39.

Parzen E (1962) On estimation of a probability density function and mode. Ann Math Stat 33:1065–76.

Pearson K, Robertson R (1981) Interneurons coactivating hindleg flexor and extensor motoneurons in the locust. J Comp Physiol [A] 144:391–400.

Perrett DI, Rolls ET, Caan W (1982) Visual neurones responsive to faces in the monkey temporal cortex. Exp Brain Res 47:329–42.

Pettersen KH, Einevoll GT (2008) Amplitude variability and extracellular low-pass filtering of neuronal spikes. Biophys J 94:784–802.

Pollack GS (1994) Synaptic inputs to the omega neuron of the cricket *Teleogryllus oceanicus*: Differences in EPSP waveforms evoke by low and high sound frequencies. J Comp Physiol [A] 174:83–89.

Pollack GS (2003) Sensory cues for sound localization in the cricket *Teleogryllus oceanicus*: Interaural difference in response strength versus interaural latency difference. J Comp Physiol [A] 189:143–51.

Pollack GS, Faulkes Z (1998) Representation of behaviorally relevant sound frequencies by auditory receptors in the cricket *Teleogryllus oceanicus*. J Exp Biol 201:155–63.

Pollack GS, Kim JS (2013) Selective phonotaxis to high sound-pulse rate in the cricket extitGryllus assimilis. J Comp Physiol [A] 199:285–93.

Popov AV, Shuvalov VF (1977) Phonotactic behavior of crickets. J Comp Physiol [A] 119:111–26.

Popov AV, Shuvalov VF, Markovich A (1976) The spectrum of the calling signals, phonotaxis, and the auditory system in the cricket *Gryllus bimaculatus*. Neurosci Behav Physiol 7:56–62.

Quiroga RQ, Nadasdy Z, Ben-Shaul Y (2004) Unsupervised spike detection and sorting with wavelets and superparamagnetic clustering. Neural Comput 16:1661–87.

Quiroga RQ, Reddy L, Kreiman G, Koch C, Fried I (2005) Invariant visual representation by single neurons in the human brain. Nature 435:1102–7.

Regen J (1913) Über die Anlockung des Weibchens von *Gryllus campestris* L. durch telephonisch übertragene Stridulationslaute des Männchens. Pflug Arch Ges Phys 155:193–200.

Reiss RF (1962) A theory and simulation of rhythmic behavior due to reciprocal inhibition in small nerve nets. In: AIEE-IRE '62 (Spring): Proceedings of the May 1-3, 1962, spring joint computer conference, pp 171–94. New York: ACM.

Richardson MJE, Brunel N, Hakim V (2003) From subthreshold to firing-rate resonance. J Neurophysiol 89:2538–54.

Roeder KD (1962) The behaviour of free flying moths in the presence of artificial ultrasonic pulses. Anim Behav 10:300–304.

Rösel von Rosenhof AJ (1749) Insecten Belustigung, zweyter Theil. Nürnberg: Fleischmann JJ.

Rosenblatt M (1956) Remarks on some nonparametric estimates of a density function. Ann Math Stat 27:832–37.

Rosenthal JJ, Bezanilla F (2000) Seasonal variation in conduction velocity of action potentials in squid giant axons. Biol Bull 199:135–43.

Sabourin P, Gottlieb H, Pollack GS (2008) Carrier-dependent temporal processing in an auditory interneuron. J Acoust Soc Am 123:2910–17.

Schildberger K (1984) Temporal selectivity of identified auditory neurons in the cricket brain. J Comp Physiol [A] 155:171–85.

Schildberger K (1988) Behavioral and neuronal mechanisms of cricket phonotaxis. Cell Mol Life Sci 44:408–15.

Schildberger K, Hörner M (1988) The function of auditory neurons in cricket phonotaxis: I. Influence of hyperpolarization of identified neurons on sound localization. J Comp Physiol [A] 163:621–31.

Schnitzler HU, Kalko EKV (2001) Echolocation by insect-eating bats. BioScience 51:557–69.

Schreiber S, Erchova I, Heinemann U, Herz AVM (2004) Subthreshold resonance explains the frequency-dependent integration of periodic as well as random stimuli in the entorhinal cortex. J Neurophysiol 92:408–15.

Schreiner CE, Langner G (1988) Coding of temporal patterns in the central auditory nervous system. In: Auditory Function: Neurobiological Bases of Hearing (Gerald M Edelman WMC W Einar Gall, ed), pp 337–61. New York: Wiley.

Schwartz O, Pillow JW, Rust NC, Simoncelli EP (2006) Spike-triggered neural characterization. J Vis 6:484–507.

Selverston AI, Kleindienst HU, Huber F (1985) Synaptic connectivity between cricket auditory interneurons as studied by selective photoinactivation. J Neurosci 5:1283–92.

Shannon CE (1948) A mathematical theory of communication. Bell Sys Tech J 27:379–423.

Sibson R (1981) A brief description of natural neighbour interpolation. In: Interpreting Multivariate Data (Barnett V, ed), pp 21–36. Chichester: Wiley.

Smith EC, Lewicki MS (2006) Efficient auditory coding. Nature 439:978–82.

Suga N (1968) Neural responses to sound in a Brazilian mole cricket. J Aud Res 8:129–34.

Sysel P, Rajmic P (2012) Goertzel algorithm generalized to non-integer multiples of fundamental frequency. EURASIP J Adv Signal Process 2012:56.

Todd BS, Andrews DC (1999) The identification of peaks in physiological signals. Comput Biomed Res 32:322–35.

Treves A (1993) Mean-field analysis of neuronal spike dynamics. Network 4:259–84.

Triblehorn JD, Ghose K, Bohn K, Moss CF, Yager DD (2008) Free-flight encounters between praying mantids (*Parasphendale agrionina*) and bats (*Eptesicus fuscus*). J Exp Biol 211:555–62.

Tuckwell HC (2005) Introduction to Theoretical Neurobiology, volume 2. Cambridge: Cambridge UP.

Tunstall DN, Pollack GS (2005) Temporal and directional processing by an identified interneuron, ON1, compared in cricket species that sing with different tempos. J Comp Physiol [A] 191:363–72.

Webb B, Wessnitzer J, Bush S, Schul J, Buchli J, Ijspeert A (2007) Resonant neurons and bushcricket behaviour. J Comp Physiol [A] 193:285–88.

Weber T, Thorson J (1989) Phonotactic behavior of walking crickets. In: Cricket behavior and neurobiology (Huber F, Moore TE, Loher W, eds), pp 310–39. Ithaca: Cornell UP.

Weber T, Thorson J, Huber F (1981) Auditory behavior of the cricket. i. dynamics of compensated walking and discrimination paradigms on the kramer treadmill. J Comp Physiol [A] 141:215–32.

Wiener N (1961) Cybernetics: Or the Control and Communication in the Animal and the Machine. 2nd edition. Cambridge: MIT Press.

Wiese K, Eilts K (1985) Evidence for matched frequency dependence of bilateral inhibition in the auditory pathway of *Gryllus bimaculatus*. Zool Jahrb Abt allg Zool Physiol Tiere 89:181–201.

Wilkins MR, Seddon N, Safran RJ (2013) Evolutionary divergence in acoustic signals: causes and consequences. Trends Ecol Evol 28:156–66.

Wohlers DW, Huber F (1978) Intracellular recording and staining of cricket auditory interneurons (*Gryllus campestris* L., *Gryllus bimaculatus* DeGeer). J Comp Physiol [A] 127:11–28.

Wohlers DW, Huber F (1982) Processing of sound signals by six types of neurons in the prothoracic ganglion of the cricket, *Gryllus campestris* L. J Comp Physiol [A] 146:161–73.

Wohlers DW, Huber F (1985) Topographical organization of the auditory pathway within the prothoracic ganglion of the cricket *Gryllus campestris* L. Cell Tissue Res 239:555–65.

Wyttenbach RA, May ML, Hoy RR (1996) Categorical perception of sound frequency by crickets. Science 273:1542–44.

Yager DD (2012) Predator detection and evasion by flying insects. Curr Opin Neurobiol 22:201–7.

Zar JH (1999) Biostatistical Analysis. 4th edition. Upper Saddle River: Prentice Hall.

Zorović M, Hedwig B (2011) Processing of species-specific auditory patterns in the cricket brain by ascending, local, and descending neurons during standing and walking. J Neurophysiol 105:2181–94.